Cover Page Information

Authors contact details

Lead Author: Dr Stephen Skinner

Department of Materials

Imperial College London

Prince Consort Road

London

SW7 2BP

Tel: +44 (0)20 7594 6782

Fax: +44 (0)20 7594 6757

Email: s.skinner@imperial.ac.uk

Co-Author: Dr Miguel Laguna-Bercero

Department of Materials

Imperial College London

Prince Consort Road

London

SW7 2BP

Tel: +44 (0)20 7594 6782

Fax: +44 (0)20 7594 6757

Email: m.laguna-bercero@imperial.ac.uk

Advanced Inorganic Materials for Solid Oxide Fuel Cells.

Stephen J. Skinner & Miguel A. Laguna-Bercero

Department of Materials, Imperial College London, Prince Consort Road, London, SW7 2BP UK

List of Abbreviations

YSZ – Yttria stabilised zirconia

ScSZ – Scandia stabilised zirconia

CGO/GDC – Gd substituted CeO_2, (Ceria gadolinium oxide or gadolinia doped ceria)

CSO/SDC – Sm substituted CeO_2 (Ceria samarium oxide or samaria doped ceria)

LSGM – $La_{1-x}Sr_xGa_{1-y}Mg_yO_{3-\delta}$

LSM – $La_{1-x}Sr_xMnO_{3-\delta}$

LSF – $La_{1-x}Sr_xFeO_{3-\delta}$

LSCF – $La_{1-x}Sr_xCo_{1-y}Fe_yO_{3-\delta}$

LSC – $La_{1-x}Sr_xCoO_{3-\delta}$

LSCM – $La_{1-x}Sr_xCr_{1-y}Mn_yO_{3-\delta}$

LSGMC - $La_{1-x}Sr_xGa_{1-y-z}Mg_yCo_zO_{3-\delta}$

LSTGM – $La_{1-x}Sr_xTi_{1-y-z}Ga_yMn_zO_{3-\delta}$

BSCF – $Ba_{1-x}Sr_xCo_{1-y}Fe_yO_{3-\delta}$

SSC – $Sm_{1-x}Sr_xCoO_2$

MIEC – Mixed ionic-electronic conductor

SOFC – Solid oxide fuel cell

TEM – Transmission electron microscopy

HRTEM – High resolution transmission electron microscopy

SAED – Selected area electron diffraction

SIMS – Secondary ion mass spectrometry

XRD – X-ray diffraction

TEC – Thermal expansion coefficient

STO – $SrTiO_3$

XAS – X-ray absorption spectroscopy

BCY – $BaCe_{1-x}Y_xO_{3-\delta}$

BZY– $BaZr_{1-x}Y_xO_{3-\delta}$

PC-SOFC – Proton conducting solid oxide fuel cell

IT-SOFC – Intermediate temperature solid oxide fuel cell

1.0 Introduction

Fuel cells are widely regarded as a next generation technology that will contribute to reductions in emissions of gases responsible for climate change such as CO_2. There are several modifications to the basic concept of a fuel cell that allow operation over a wide variety of temperatures and with differing fuels. One of the most promising types of fuel cell for large scale power generation and combined heat and power applications is the solid oxide fuel cell (SOFC). The solid oxide fuel cell offers many advantages over conventional combustion-based power generation technologies and has been the subject of intensive investigation for many years. As with all other fuel cells the SOFC is an electrochemical energy conversion device that converts the chemical energy contained within a fuel (for example, H_2) to useful electrical energy through an electrochemical oxidation process. Using the simplest fuel as an example the overall chemical reaction occurring is:

$$H_{2(g)} + {}^{1}\!/\!_{2}\, O_{2(g)} \rightarrow H_2O_{(g)} \qquad (1.0)$$

To achieve this overall reaction it is essential that we consider the basic components of the fuel cell. A SOFC consists of three ceramic functional components (anode "fuel side", cathode "air side" and electrolyte) plus an electrical interconnect that is either ceramic or metallic depending upon the operating environment. These

components are referred to as the fuel cell and to achieve suitable power outputs these individual cells are connected to form a fuel cell stack. Schematics of two alternative designs of a single fuel cell are shown in Figure 1.

At the anode the fuel is oxidised with the oxidant (oxygen) reduced at the cathode. These two components are separated by a gas tight electrolyte membrane that is a pure ionic conductor, transporting the oxide ion species from the cathode to the fuel side. This process releases electrons to an external circuit, providing the useful electrical power. These reactions are summarised as:

cathode reaction $$\tfrac{1}{2}O_{2(g)} + 2e^- \rightarrow O^{2-} \qquad (1.1)$$

anode reaction $$H_{2(g)} + O^{2-} \rightarrow H_2O_{(g)} + 2e^- \qquad (1.2)$$

Evidently these electrode reactions are significantly more complex than shown in equations 1.1. and 1.2 and fuller discussions of the proposed fuel oxidation and oxygen reduction electrode reactions are given in [1-4].

It is therefore clear that in a solid oxide fuel cell there are many processes that require optimised materials, and consequently the SOFC is a complex solid state device. As a summary, it is essential that the electrolyte is a gas tight, pure ionic conductor stable over a wide pO_2 range (>10^{-24} atm). Anodes have to possess stability in reducing conditions with both high ionic and electronic conductivity, and chemical compatibility with the electrolyte material. Similar properties are required for the cathode with the exception that stability is now in oxidising environments. Additionally the cathode has to be catalytically active towards oxygen reduction, which is often a rate limiting process, particularly at lower temperatures of operation (<650 ^{o}C). These are demanding properties for a set of materials and have led to a relatively small number of materials finding application in solid oxide fuel cells.

Several excellent reviews[5-11] have reported on the development of conventional solid oxide fuel cell materials and these details will only be briefly summarised here.

1.1 Conventional solid oxide fuel cell electrolytes

A solid oxide fuel cell was proposed by Baur and Preis[12] as far back as 1937 based upon an electrolyte of stabilised zirconia with metallic electrodes. Since then stabilised zirconia has been the electrolyte that has received most attention by fuel cell developers. Most zirconia electrolytes are based upon either yttria or scandia stabilisation of the tetragonal polymorph[6, 7, 13], commonly referred to as YSZ and ScSZ respectively, although a number of alternative dopants have been investigated, Table 1. Conventionally the substitution level is between 3 and 8 mol % for the yttria based materials and at 10-12 mol% for the Sc based materials. The choice of the dopant level is dictated by a compromise between mechanical robustness and overall conductivity, as summarised in Table 1. Substitution of zirconia results in the stabilisation of either the tetragonal or cubic polymorphs adopting the fluorite type structure as shown in Figure 2. This substitution also provides an increased concentration of oxygen vacancies within the lattice facilitating increased ionic conductivity, as illustrated by the incorporation reaction below:

$$Y_2O_3 \xrightarrow{ZrO_2} Y'_{Zr} + V_O^{\bullet\bullet} + 3O_O^x \qquad (1.3)$$

One significant disadvantage with the ZrO_2 based SOFCs is the temperature of operation at which ionic conductivity is sufficiently high support a device which for 8YSZ is typically 800-1000^{o}C, depending upon the thickness of the electrolyte. This leads to a further consideration for fuel cell operation – that of electrolyte supported or electrode supported designs. Again each design has advantages, but to increase performance it is generally accepted that lower operating temperatures are required

and thus thinner electrolytes. As electrolyte thickness decreases to below 100μm self-supporting electrolytes are no longer mechanically feasible. Hence the deposition of layers of dense electrolytes on porous electrodes becomes a significant processing issue. On moving to a Sc based system it is possible to achieve greater conductivities at lower temperatures than with YSZ thus reducing the operating temperature of the fuel cell.

Despite the relatively low levels of conductivity displayed by zirconia based electrolytes these materials have the major advantage of exhibiting considerable chemical stability as a function of oxygen partial pressure, presenting no degradation at a pO_2 as low as 10^{-24} atm. However there are some further considerations when using ZrO_2 based cells, including the reactivity of the electrolyte with cathodes and the necessity to use exotic alloys or high cost interconnect ceramics, combined with issues surrounding cell sealing. For these reasons two other types of electrolyte have been developed – lanthanum gallate based perovskites and ceria based fluorites.

Ceria based electrolytes have been proven to operate at much reduced temperatures (500-700 ^oC) with ionic conductivity comparable to YSZ at much higher temperatures[14, 15]. Commonly the CeO_2 host is substituted with either Sm or Gd ($Ce_{1-x}Sm_xO_{2-\delta}$, CSO, and $Ce_{1-x}Gd_xO_{2-\delta}$, CGO), creating significant vacancy concentrations. Use of these ceria based materials is limited by the redox characteristics of the $Ce^{3+/4+}$ couple, with reduction occurring at temperatures above about 650 ^oC leading to a reduction of the ionic transport number. This in turn can lead to short circuits within the cell and hence a loss of performance. However, as conductivity in ceria based compounds is sufficient at temperatures below 650 ^oC for fuel cell electrolytes, the issue is then one of suitably active cathodes, addressed in section 1.3 below.

The final class of “conventional” electrolyte is based upon the perovskite structured (ABO_3) lanthanum gallate, Figure 3. Ishihara[16-20] and Goodenough[21-24] both reported

in the 1990's fast oxide ion conduction in doubly substituted gallates, giving a composition of $La_{1-x}Sr_xGa_yMg_{1-y}O_{3-\delta}$ (LSGM) where x = 0.1 or 0.2 and y = 0.2. Levels of conductivity reported were higher than the YSZ materials in the 600-750 ^oC temperature range. Figure 4, and consequently received significant attention. Further reports indicated that a minimal Ni or Co content on the B site enhanced the ionic conductivity further[25, 26]. Many authors have attempted to optimise the LSGM type electrolytes and further details of these novel electrolytes will be discussed in section 2.1.1. Given the optimal operating temperatures of the three electrolytes detailed above it is clear that there are three main operating regimes for solid oxide fuel cells: 500-650 ^oC, 650-800 ^oC and 800-1000 ^oC, with regimes corresponding to ceria-based, LSGM-based and ZrO_2-based electrolytes respectively. Each of these regimes required the development of specific electrodes optimised (or compromised?) for the operating temperature and these electrodes are discussed in the subsequent sections.

1.2 Conventional anodes

In SOFCs the composition of the anode is limited to a large extent by the stringent requirements placed upon the material, including oxide ion mobility, high electronic conductivity, catalytic activity for hydrogen oxidation and stability at very low pO_2. Typically anodes in SOFCs will operate under a gas mixture containing CH_4/H_2O rather than a pure H_2 fuel stream. This is possible as the typical cermet of Ni/YSZ exploits the catalytic activity of Ni for steam methane reforming, forming a hydrogen rich syngas that can then be oxidised electrochemically. As a consequence of this there are currently very few "conventional" anode materials to choose from. In general the anode is a composite material consisting of a metallic component mixed with the electrolyte composition. Hence for YSZ-based cells the anode material

would typically be of Ni-YSZ composite type[27, 28]. These composites are often referred to as “cermets”. Similarly for CGO and LSGM based cells the composite materials are of the Ni-CGO and Ni-LSGM type.

Preparation of the anode structure is usually achieved through the mixing of NiO with the appropriate electrolyte component, followed by a reduction step to produce the Ni cermet. Volume changes associated with the reduction step do not appear to be detrimental to the overall durability of the cell, but there have been observations of serious degradation of the anode when reoxidation occurs. These are significant concerns for thermal cycling and it is clear that over relatively modest timescales there is a significant degradation rate of 10mΩ cm^{-2} per 1000 hours at 1000 ^{o}C for YSZ based devices[29]. Clearly these degradation rates and the evolution of reaction products is too great for long term operation. Redox stability of the electrode structure is therefore a common problem for Ni based anodes, and significant volume changes upon oxidation of Ni to NiO have been demonstrated to significantly impact upon the mechanical integrity of the cell[30].

One further limitation of the anode component in these devices is the degradation of performance with the increase of sulphur content in the fuel stream and also with the risk of coking if carbon rich fuel streams are used, such as with natural gas[31]. Evidently if a pure hydrogen fuel were used in the SOFC these issues of anode operation would not arise, however one of the advantages of the SOFC is the potential fuel flexibility offered by the use of oxide anodes, such as the reforming of natural gas in the anode.

1.3 Conventional cathodes

Cathode materials for SOFCs based on any of the electrolytes described in section 1.1 are of the perovskite structure type, generally La-based with transition metals located on the B site. Several authors[4, 5, 32-35] have summarised the range of

perovskites investigated to date, concentrating on the conductivity, ion transport and compatibility of these materials. As such it is superfluous to continue the discussion in detail here. Instead we will refer to the main cathode types only, leaving the reader to consult the relevant literature for further details.

The majority of SOFC cathodes are based upon either $LaMnO_3$ or $LaCoO_3$ substituted with Sr on the A-site and Fe on the B-site. The rationale for using these materials is a result of the best compromise in properties for the cathodic reactions. In general, with higher temperature cells, such as those based on YSZ, the cathode functions as a triple phase boundary (TPB) material, where the chemical reactions between the electrode, electrolyte and gas phase take place at a limited area within the cathode structure, Figure 5. In this case the electrode material is functioning as an electronic conductor and oxygen reduction catalyst. For this case the Sr doped $LaMnO_3$ (LSM) is a suitable choice with conductivity of the order of 320 Scm^{-1} at 800 ^oC[36] for the $La_{0.6}Sr_{0.4}MnO_3$ composition. Whilst LSM acts as a suitable electrode at these elevated temperatures, there are some fundamental issues with this cathode material that compromise its performance, including the reactivity of LSM with YSZ to form insulating interfacial reaction products of the pyrochlore type, $La_2Zr_2O_7$[37, 38]. This is clearly detrimental to the overall performance of the cell as this reaction product acts as a blocking phase for the cathode reactions.

On reducing the temperature of operation we find that the performance of the LSM cathode with respect to oxygen reduction and surface exchange is no longer sufficient. Indeed at the lower temperatures where CGO is used as the electrolyte it becomes necessary to move away from the triple phase boundary model and use materials that are both ionic and electronic conductors (MIEC – mixed ionic electronic conductor) effectively extending the TPB over the entire cathode surface. On replacing Mn with Co it is noted that a material with both high electronic conductivity and fast ion conductivity is produced, $La_{1-x}Sr_xCoO_{3-d}$ (LSC). However the thermal

properties of this composition are such that a significant mismatch in the thermal expansion coefficients proves detrimental to performance as thermal cycling results in cracking and delamination of the cathode. To overcome this issue a substitution of Fe for Co was performed and a resulting decrease in thermal expansion coefficient observed[39, 40]. Unfortunately this substitution also resulted in a reduction of the MIEC properties of the cathode. Hence, to promote cathode performance at lower temperatures, composite cathodes of $La_{1-x}Sr_xCo_{1-y}Fe_yO_{3-d}$ (LSCF) with CGO have been produced[41].

On LSGM electrolytes similar cathodes have been developed with perhaps some of the most exciting recent results focussing on the $Ba_{1-x}Sr_xCo_{1-y}Fe_yO_{3-d}$ (BSCF)[42-50] and $Sm_{1-x}Sr_xCoO_{3-d}$ (SSC)[51-55] compositions. The development of these materials has resulted from the continued interest in substitution of both the lanthanide and transition metal components in the perovskite lattice. A more detailed discussion of these new cathode materials in operation with LSGM, YSZ and CGO electrolytes is given in section 2.2.

1.4 Summary

In the preceding sections the main materials currently used in solid oxide fuel cells have been detailed along with the background regarding the materials requirements controlling application of these oxides. It is clear that the SOFC is a complex all ceramic device with many challenges to overcome before a truly robust device can be marketed. In the subsequent sections we outline the main materials developments in terms of new compositions and structure types that will compete for inclusion in next generation devices with enhance performance and durability. In this we include the potential for development of proton conducting ceramic fuel cells.

2.0 Next Generation SOFC materials

Whilst SOFCs have developed significantly over the past few decades the main focus of materials development has been on the fluorite- and perovskite-based functional components. Each of the materials selections discussed above has deficiencies and there is now considerable effort directed towards the development of novel materials and structures with better performance for next generation SOFCs. In the following sections the potential choices available for low temperature electrolytes and cathodes and sulphur tolerant anodes will be discussed.

2.1 Novel electrolyte materials

2.1.1 Electrolytes based on ABO_3 perovskite

Initial studies of the oxide ion conductivity of materials with the ABO_3 perovskite structure were reported by Takahashi and Iwahara[56] in solid solutions such as $CaTi_{1-x}$-$Al_xO_{3-\alpha}$, $CaTi_{1-x}$-$Mg_xO_{3-\alpha}$ and $SrTi_{1-x}$-$Al_xO_{3-\alpha}$. Relatively recently, perovskite and related crystal structures have been investigated and proposed as good oxide ion conductors, as presented in Table 2. The highest overall bulk oxide ion conductivity was reported for the $La_{0.8}Sr_{0.2}Ga_{0.83}Mg_{0.17}O_{3-\delta}$ (LSGM) composition. At 800 ºC this material presents a conductivity of 0.166 S cm^{-1}, which is approximately 4 times the conductivity of YSZ at the same temperature,[22] and is therefore considered as a potential candidate for intermediate temperature SOFC (IT-SOFC) applications.

Apart from its good conductivity, higher than that of both YSZ and ScSZ and similar to that of GDC, Sr and Mg doped $LaGaO_3$ (LSGM) is stable in both fuel and air, and especially at low oxygen partial pressures, where GDC is easily reduced as redox of the Ce^{4+}/Ce^{3+} couple is facile. It was also noted that the conductivity of LSGM depends strongly on the dopant concentration as shown in Figure 6.

In order to improve the conductivity of LSGM several approaches involving the addition of dopants on both A and B sites have been suggested. Partial substitution (10 mol %) of the La site by other rare earth ions such as Nd, Sm, Gd, Y and Yb in the $La_{0.9}Sr_{0.1}Ga_{0.8}Mg_{0.2}O_{2.85}$ composition was however found to decrease the total electrical conductivity[17,57]. The lanthanum site can also be substituted with barium[58] as an alternative to Sr and on substitution with barium it was observed that the octahedral tilt angle was affected reducing the activation energy for conduction. $La_{0.9}Ba_{0.1}Ga_{0.8}Mg_{0.2}O_{2.85}$ (LBGM) presents lower conductivity than LSGM at high temperatures but conversely presents higher conductivity values at lower temperatures[59], thus making the material of interest for lower operating temperature devices. It has also been shown that replacement of Sr^{2+} ions by K^{+} ions in LSGM decreases the electrical conductivity of LSGM and increases the activation energy whereas the substitution of La by substantial amounts of up to 50 atom % of Pr in LSGM does not affect the electrical conductivity[60]. Hence A site substitution appears to be detrimental to overall conductivity in the LSGM type electrolytes.

The effect of B-site substitution has been also widely studied. Partial substitution of Ga by Al or In also decreases the electrical conductivity of LSGM. This decrease may be attributed to changes in the crystal structure and lattice parameter[61]. However, Pr and In co-substitutions forming the composition $La_{0.4}Pr_{0.4}Sr_{0.2}In_{0.8}Mg_{0.2}O_{2.8}$ results in high electrical conductivity at low temperatures with a remarkably low activation energy of only 0.44 eV. This increase in the electrical conductivity has been suggested to be due to the higher number of oxygen vacancies or an increase in the electronic conductivity due to the mixed valence of Pr[61]. The addition of transition metals, such as cobalt[25, 62-64] and iron,[62,65] were found to increase the conductivity of LSGM, especially at low temperatures as shown in Figure 7. Small additions of Fe or Co increase the electrical conductivity at low temperatures due to the introduction of electronic charge carriers into the lattice. However, at high temperatures the total

conductivity is dominated by ionic conduction, being similar to that of LSGM. Therefore, the addition of transition metals such as Fe or Co into LSGM does not have a significant effect on the ionic conductivity. On the contrary, high doping levels might yield LSGM-based compositions for use as SOFC cathodes. The use of nickel as a dopant for LSGM has also been reported, presenting similar results to those observed with cobalt substitution[66].

In order to produce high quality electrolyte powders interest has been directed towards novel preparation methods of the LSGM compositions to ensure high homogeneity, good sinterability and enhanced performance. For example, $La_{0.9}Sr_{0.1}Ga_{0.8}Mg_{0.1}Co_{0.1}O_{2.85}$ (LSGMC) powders have been synthesized by carbonate co-precipitation resulting in the ionic conductivity of the LSGMC samples increasing to 1.13 Scm^{-1} at 800 ^oC[67]. Further preparation methods recently developed for LSGM and LSGMC are sol-gel synthesis[68] and spark plasma sintering[69], with the latter technique used to reduce the sintering temperature and time taken to produce gas tight, high density membranes.

2.1.2 Other perovskite-based derivatives

Other potential electrolytes with the perovskite-type structure are the $SrSn_{1-x}Fe_xO_{3-\delta}$ ($0<x<1$) compositions or Ga and Sc doped $CaTiO_3$. It has been found that solid solutions of $SrSn_{1-x}Fe_xO_{3-\delta}$ with low Fe contents (<0.3) exhibit regimes of predominant ionic and electronic conductivity. For example, $SrSn_{0.9}Fe_{0.1}O_3$ exhibits p- and n-type electronic conductivity at high and low oxygen partial pressures respectively[70]. Ga and Al doped $CaTiO_3$ samples also present p- and n-type electronic conductivity at both high and low oxygen partial pressures, while $CaTi_{0.9}Sc_{0.1}O_{3-\delta}$ shows predominantly ionic conductivity over a wide range of oxygen partial pressures at a temperature of 800 ^oC[71].

2.1.3 Electrolytes based on $La_2Mo_2O_9$ (LAMOX)

Lanthanum molybdate, $La_2Mo_2O_9$, has been reported to exhibit fast oxide-ion conducting properties comparable with the conventional zirconia and ceria compositions[72]. This compound presents a different crystal structure from all known oxide electrolytes, and consists of isolated $(MoO_4)^{2-}$ units in a three-dimensional matrix of $(La_2O)^{4+}$. $La_2Mo_2O_9$ undergoes a reversible phase transition from the non-conductive monoclinic α-form to the highly conductive cubic β-form at approximately 580 ^oC. Powder X-ray diffraction (XRD) of the phases *α* and *β* are practically identical, because the structural phase transition *α* → *β* is actually a transition from a static to dynamic distribution of the oxygen defects without any shift of the heavy atoms[73]. High-resolution XRD is however required to reveal the structure of the monoclinic *α*-phase, a complex structure suggested to comprise 312 non-equivalent atoms[74]. The complex structure of the monoclinic phase is viewed as impeding the oxygen ordering underlying the *β* → *α* phase transition.

In Figure 8 ionic conductivity data is presented and compared with that of stabilized zirconia. The high-temperature phase, β-$La_2Mo_2O_9$, has a cubic structure which is derived from that of β-$SnWO_4$, Figure 9. Partial site occupation by oxygen atoms, strongly anisotropic thermal factors, and short-range order with a distance characteristic of O-O pairs has been evidenced[75]. A structural model for the origin of the oxygen ion conduction in β-$La_2Mo_2O_9$ based on the β-$SnWO_4$ compound has been proposed. It was suggested that the substitution of a lone pair cation (Sn^{2+}) by a non-lone pair one with higher oxidation state (e.g. La^{3+}) could be used as a model to design new fast oxide ion conductors[76].

In order to stabilize the β-structure at lower temperatures, suppressing the α-β phase transition, minor doping of $La_2Mo_2O_9$ has been found to be effective[77]. For example, substitution of W for Mo has been shown to stabilize the β-phase at room temperature with Collado et al.[78] reporting that $La_2W_{2-x}Mo_xO_9$ can be prepared as

single β-phase at any cooling rate for compositions where x ≥ 0.7. Small additions of niobium were found to increase the conductivity when compared with the undoped $La_2Mo_2O_9$ phase[79, 80].

Substitution of Nd, Gd and Y for La has also been studied with gadolinium and yttrium both found to stabilize the cubic β phase at room temperature. Gd and Y substitutions also seem to increase anion conductivity of the β phase[81]. Small amounts of Ba doping were also found to increase the overall conductivity of the parent compound $La_2Mo_2O_9$ to a notable extent both at low and high temperatures[82]. Other dopants substituting for lanthanum (Ca^{2+}, Sr^{2+}, Ba^{2+} or K^{+}) have also been studied[83]. Although these substitutions do not improve the ionic conductivity compared to the intrinsic vacancies in the structure, an increase of the redox stability, essential for SOFC applications in the low-temperature range for these materials was observed.

A series of optimised $La_2Mo_2O_9$ materials have been studied using the isotope exchange depth profile technique and secondary ion mass spectrometry (SIMS) analysis. Oxide ion diffusion coefficients (D*) in both the parent compound and optimised materials were found to be significantly higher than those reported for any of the fluorite structured electrolyte materials, obtaining the best value for the $La_{1.7}Gd_{0.3}Mo_2O_9$ composition of $D^* = 1.41 \times 10^{-6}$ cm^2 s^{-1} at 800 ^oC[84]. These diffusion coefficients obtained for stabilised compositions indicates the potential for use as intermediate temperature SOFC electrolytes, assuming that the durability and compatibility with electrodes are proven competitive with existing zirconia and ceria based systems.

Recently, different preparation methods, such as spark-plasma sintering[85], thermal processing methods[86] or polyaspartate precursor methods[87], have been shown as potential synthesis methods in order to improve the ionic conductivity of $La_2Mo_2O_9$

based electrolytes. As previously, these techniques optimise the particle morphology and homogeneity resulting in improved performance.

2.1.4 Brownmillerite structured oxides and derivatives

The $A_2B_2O_5$ brownmillerite structure is derived from the ABO_3 cubic perovskite structure in which half of the anions have been removed from alternate BO_2 layers. This gives the stacking sequence *A*O–*B*O_2–*A*O–*B*O–*A*O– with alternating layers of apex-linked *B*O_6 octahedra and *B*O_4 tetrahedra as shown in Figure 10. The oxygen vacancies are ordered along (010) planes and they may contribute to ionic transport forming one-dimensional diffusion pathways for oxygen ion migration in the tetrahedral layers[88]. Electrical conductivity is typically oxygen-ionic in dry atmospheres with moderate oxygen partial pressures, mixed ionic and p-type electronic under oxidizing conditions, and protonic under gas mixtures containing H_2O. The parent compound, $Ba_2In_2O_5$, presents mixed conductivity with dominant oxygen transport in dry air and at room temperature has orthorhombic symmetry. A transition into the tetragonal polymorph disordered perovskite phase at above 925 ^oC is reported, which leads to a dramatic increase of the ionic conduction[88]. At 1040 ºC, $Ba_2In_2O_5$ transforms into a disordered cubic phase which is a pure oxide ion conductor. In order to stabilize the disordered cubic perovskite structure and thus to increase the ionic transport in the intermediate temperature range, substitution of indium with higher-valence cations, such as Zr^{4+}, Ce^{4+} or Sn^{4+} has been studied[89, 90]. Total conductivity of $Ba_2In_2O_5$ and other related compounds is presented in Figure 11, and compared with 8 mol% YSZ[91].

Doping of $Ba_2In_2O_5$ with Co has been investigated forming the $BaIn_{0.9}Co_{0.1}O_{3-\delta}$ composition (cubic perovskite structure) and shows high oxide ionic conductivity comparable to the original $Ba_2In_2O_5$ and high electronic conductivity. For example, at 850 ^oC the sample presents a total conductivity of 4.7×10^{-1} S cm^{-1} and an oxide ion

transport number of 0.52 at 850 °C[92] disqualifying this composition from consideration as an electrolyte. Partial substitution for In in $Ba_2In_2O_5$ with V, Mo and W also led to the stabilisation of the fast oxide ion conducting cubic form at lower temperatures. As for substitution by cations with a smaller radius than that of In^{3+}, a decrease of the order–disorder transition temperature with the increased level of substitution is reported, and it is associated with a decrease in the conductivity[93]. Below 400 °C, an uptake of water is observed for all of the materials, which makes them promising as potential proton conductors. Further partial substitutions on the In site including Cu[94], Ga[95], Y[96], Ti[97], Sc, Ta, Nb or Si[98], and Sr[99] or La[99,100] , as a substitution for Ba, also stabilize the cubic perovskite phase at low temperatures.

2.1.5 Bi_2O_3 based electrolytes

δ-Bi_2O_3 is renowned as the best oxide ion conductor with conductivity 1-2 orders of magnitude higher than the best performing YSZ. A phase transition from the monoclinic α-phase to the highly conductive cubic δ-phase at about 730 °C was first reported by Gattow *et al*.[101], who noted that the δ-phase was stable up to its melting point of approximately 825 °C. They also performed high temperature power X-ray diffraction, showing that the δ-phase crystallized in a fluorite-type cubic cell (space group *Fm-3m*) with a ¼ defective anionic *8c* Wyckoff site. Neutron diffraction studies at 778 °C[102] allowed precise determination of the structural disorder, with the oxygen ions in 8c and 32f sites and partial occupancy factors fitting to the total oxygen content. This disorder of oxide ions is viewed as being responsible for the observed fast oxide-ion conduction. Unfortunately δ-Bi_2O_3 suffers from significant instability in reducing environments leading to electronic conduction, and hence this discounts the parent phase from serious consideration as an electrolyte. In an effort to instigate stabilisation of the δ-phase at lower temperatures substitution of bismuth with other

dopants has been attempted by many authors. Of the species used for stabilisation Y_2O_3[103-105] and rare earth oxides Er_2O_3[106, 107], Dy_2O_3[108], Sm_2O_3[109] or Yb_2O_3[110] have been most prevalent. It has also been found that stabilization of the fcc phase is possible by substituting with higher valent dopants such as M_2O_5 (M= V, Nb, Ta)[111] or WO_3[112].

Another interesting system is Bi_2O_3-Gd_2O_3[103, 109], which adopts both the cubic and rhombohedral phases depending upon composition, both being good oxygen ionic conductors. In general, it is found that the rhombohedral phase is formed in the case of relatively large M^{3+} ions, and the cubic structures are usually formed in the case of a relatively small cationic radius[113]. Iwahara *et al.*[114] showed the formation range of the cubic and rhombohedral phases as a function of the ionic radius in the Bi_2O_3-M_2O_3 system, as presented in Figure 12. It is clear from this that using dopants with small cationic radius facilitates the stabilization of the cubic phase.

Further studies of La_2O_3 doping of Bi_2O_3 indicates that a rhombohedral ε-structure exists and that this presents the highest conductivity of all bismuth oxide based systems[115, 116]. In Figure 13 we present the relative performance of different compositions of doped bismuth oxide samples compared to a standard YSZ electrolyte[117] indicating the attractive performance of this class of materials if purely ionic conductivity is considered.

Moreover, Watanabe reported that all δ-phases reported at room temperature were metastable[118, 119], claiming that all of the stabilized δ-phases reported were nothing but the quenched high-temperature phases which form solid solutions based on δ-Bi_2O_3. These quenched phases are obtained in the bismuth-rich region of a system with Ln_2O_3 (Ln = lanthanoid), Y_2O_3, TeO_2, Nb_2O_5 or Ta_2O_5. On annealing at low temperatures (below approx. 700 ^oC) they transform gradually to the low-temperature

stable modification in the systems with Ln_2O_3, or decompose into two other phases in the other systems, to yield far lower electrical conductivities[120, 121].

More recently, it has been demonstrated that stabilization of the δ-phase in ternary systems, such as Bi_2O_3-Er_2O_3-WO_3[122], Bi_2O_3-ZrO_2-Nb_2O_5[123], Bi_2O_3-ZrO_2-Y_2O_3 or Bi_2O_3-Nb_2O_5-Ho_2O_3 solid solutions[124] is possible, leading to the formation of new oxide-ion conductors. These ternary systems appear to be more stable in comparison with the metastable binary systems. For example, the $(Bi_2O_3)_{0.705}(Er_2O_3)_{0.245}(WO_3)_{0.05}$ system shows no degradation up to 1100 hours at 600 ºC[122] and has led to consideration of a new class of ion conductors discussed in the following section.

To improve performance as an electrolyte, thin films of *δ*-Bi_2O_3 have been synthesized by Laurent *et al.*[125]. These authors believe that the small crystallite size (~10-15 nm) achieved through this preparation route might explain the stability of the metastable phase at low temperature, as they achieve a conductivity of about 0.39 Scm^{-1} at 440 ^oC. Although this high conductivity value is very promising, further work is required in order to probe the stability of these thin films.

2.1.6 Novel materials based upon Bi_2O_3 and $Bi_4V_2O_{11}$

As previously described, bismuth oxide has high ionic conductivity but also presents several disadvantages, including thermodynamic instability at low oxygen partial pressures, volatilization at moderate temperatures, high corrosion activity and low mechanical strength.

Alternative bismuth based materials have been investigated with the aim of exploiting the high oxide ion conductivities of the defect fluorites whilst stabilising the material to lower temperatures and wider pO_2 ranges. Mauvy *et al.*[126] studied compounds of the general formula $Bi_{18-4m}M_{4m}O_{27+4m}$ where the variable *m* ($0 \leq m \leq 1$) defines the ratio of the number of $[Bi_{14}M_4O_{31}]$ over the total number of layers in the sequence. Two new

compounds were reported: $Bi_{14}P_4O_{31}$ and $Bi_{50}V_4O_{85}$. These materials present monoclinic symmetry and are characterized by cationic ordering of bismuth and the *M* atoms (*M* = P, V) in the framework. $Bi_{14}P_4O_{31}$ unfortunately is not a good ionic conductor but the related $Bi_{50}V_4O_{85}$ presents a conductivity of 0.001 Scm^{-1} at 650 ^oC and has an activation energy of 1.05 eV, close to that of YSZ (~1 eV).

By double doping with rhenium and a rare earth cation (RE = La, Nd, Eu, Er, and Y), the *δ*-Bi_2O_3 can be stabilized using even the largest lanthanides, a phenomenon not previously reported, and some compositions show significantly higher conductivities at low temperatures (<400 ^oC) than other *δ*-Bi_2O_3 phases[127]. For example, the conductivity of $Bi_{12.5}La_{1.5}ReO_{24.5}$ at 300 ^oC is about one order of magnitude higher than for phases stabilized by joint Dy/W substitutions, which were previously reported to exhibit the highest conductivities[128], and also approaches that of the best low-temperature conductor, the 2-dimensional $Bi_2V_{0.9}Cu_{0.1}O_{5.35}$ (BICUVOX)[129], as presented in Figure 14.

Of recent interest are also the solid solution compositions $Bi_{5-x}Ln_xNbO_{10}$[130]. These composition exist up to a value of approx. *x* = 0.25 for La, and to *x* = 0.5 for Gd and Y. Except for Bi_5NbO_{10}, which appears to be a pure ionic conductor, most of the solid solutions exhibit mixed conductivity with predominant ionic transport. Partial Gd and Y substitutions favour electron conductivity in the low temperature range, probably due to bismuth partial oxidation, indicating that electrode applications may be possible, but that again these materials are unsuitable for electrolytes without substantial optimisation.

Another important family of materials based on Bi_2O_3 are those that adopt the Aurvillius type structure (perovskite-related layered structure) with the chemical formula $Bi_4V_2O_{11}$, firstly reported by Abraham *et al.*[131] The low temperature phase is α-$Bi_4V_2O_{11}$, and it presents two reversible phase transitions at 450 ^oC (β-phase) and

570 °C (γ-phase). The high temperature γ-$Bi_4V_2O_{11}$ exhibits fast oxide ionic conductivity of about 0.1 Scm^{-1} at 600 °C, where the oxygen vacancies are disordered[89]. The crystal lattice of the doped γ-vanadate (BIMEVOX) family consists of alternating $Bi_2O_2^{2+}$ and perovskite-like $VO_{3.5}^{2-}$ layers, with oxygen vacancies in the perovskite layers providing ion migration. Aliovalent cations have been used to stabilize the γ-phase at room temperature. Solid solutions of $Bi_2V_{1-x}MO_{5.5-\delta}$ (M= Cu, Ni and $0.07 \leq x \leq 0.12$) have some of the highest oxygen ionic conductivities reported for this class of materials[132] and, for example, $Bi_4V_{1.8}Cu_{0.2}O_{10.7}$ exhibits a conductivity of 10^{-3} Scm^{-1} at 300 ºC, which is approximately two orders of magnitude higher than that of the pure $Bi_4V_2O_{11}$[133]. Despite the reasonably high conduction, the use of Aurivillius phases for electrochemical applications is restricted due to their high chemical reactivity and low mechanical strength[134].

2.1.7 Apatite structure oxides

Oxyapatite materials adopt the general formula $A_{10}(MO_4)_6O_{2\pm\delta}$, where A is a rare-earth or alkaline earth cation and M is a p-block element such as P, Si or Ge. Their structure consists of isolated MO_4 tetrahedra arranged so as to form oxide-ion and A channels parallel to the *c* axis, with the oxide-ion channels being central to the oxide ion conductivity, as shown in Figure 15[135].

White *et al.*[136] have proposed an alternative description of the apatite structure. They have shown that apatites can be simply described as zeolite-like microporous frameworks ($A_4(MO_4)_6$) composed of face-sharing AO_6 trigonal prismatic columns, that are corner connected to the MO_4 tetrahedra. These frameworks allow flexibility to accommodate the $A_6O_{2\pm\delta}$ units and indicate how the oxygen interstitial excess can easily be accommodated in the structure.

Alternative rare-earth apatite materials have been proposed recently as solid electrolyte materials due to the discovery of fast oxide-ion conductivity in the silicate-

based apatite systems[137-141]. A recent computer modelling study by Tolchard *et al.*[142] indicates that an unusually broad range of dopant ions (in both size and charge state) can substitute for La in the $La_{9.33}Si_6O_{26}$ apatite. The range of dopants is much wider than that observed for doping on a single cation site in most other ionic conductors for fuel cell applications, such as the perovskite-type oxides. The observed conductivity is very sensitive to the doping regime and cation-anion non-stoichiometry. However, the highest conductivities are found for the oxygen-excess samples, with oxide-ion conduction occurring mainly along the oxide-ion channels. There is a wide range of doping possibilities in both the lanthanum site (Mg, Ca, Sr, Ba, Co, Ni, Cu, Mn, Bi) and the silicon site (B, Al, Ga, Zn, Mg, Ti, Ge, Fe, Co, Ni, Cu, Mn, P), as reported by Kendrick *et al*[135] and references therein, giving considerable scope for future development.

In order to study the conduction mechanism of oxygen ion migration, atomistic modelling studies have been performed[143], suggesting that the high ionic conductivity in the apatites of non-stoichiometric composition is mediated by oxygen interstitial migration along the c-axis and involving cooperative displacements of the SiO_4 tetrahedra. The predicted location of the interstitial next to the SiO_4 tetrahedra has been confirmed in the oxygen excess samples by structural studies[144] and spectroscopic techniques such as ^{29}Si NMR[145] and Raman spectroscopy[146]. In samples with cation vacancies, the conduction is found to be mediated by Frenkel-type interstitial oxide ions[146-148].

Water incorporation in $La_{9.33+x}(Si/GeO_4)_6O_{2+3x/2}$ has also been reported leading to an enhancement of the total conductivity[149]. According to the authors, they attributed this increment to proton conduction at temperatures below 600 K in wet atmospheres. Little further work has been reported on the nature of this proton conduction, but it is evidently of significance when contemplating applications.

One of the drawbacks with the apatite ceramics, is that despite their good conductivity synthesis of gas tight membranes has generally required temperatures in the range 1600-1750 ^{o}C. Evidently to implement these materials a significant reduction in sintering temperature is required. To achieve this Chesnaud *et al.* have used novel sintering and synthesis routes to produce fully dense apatite silicate ceramics through a combination of freeze-drying and spark plasma sintering[150]. This results in a reduction in synthesis temperature of fully dense membranes to temperatures as low as 1200 ºC which is then competitive with processing conditions of conventional electrolytes.

High oxide-ion conductivity has also been reported in the germanium based systems, showing higher activation energies that the analogous silicates[151]. Although higher levels of oxygen excess can be achieved in the germanates, the samples with high hyperstoichiometry show the additional complexity of a change in the crystal symmetry from hexagonal to triclinic, with an associated decrease in the conductivity at low temperatures[141, 152].

Regarding doping strategies for the Ge-based materials, substitution on the La site with divalent cations such as Ba, Sr, Ca, Mg, Cu, Ni, Mn or Co, helps to stabilise the more conductive hexagonal lattice, whereas doping on the Ge site with Co, Al or Ga tends to stabilise the triclinic symmetry[153]. However, the fact that the conductivities in the hexagonal germanate systems appear to be less sensitive than the silicates to the effect of the dopants or the dopant site may indicate a range of conduction pathways. In this trend, Kendrick *et al.*[154] have reported some atomistic simulation work on $La_{9.33+x}(GeO_4)_6O_{2+3x/2}$, showing the migration of interstitial oxide ions via the GeO_4 tetrahedra both parallel and perpendicular to the c-axis. These interstitial sites lead to the consequent formation of Ge_2O_9 units with the presence of five-coordinated germanium, also proposed by Pramana *et al*.[155].

Finally, Tsipis *et al.* have studied the integration of the $La_{10}Si_5AlO_{26.5}$ electrolyte with different cathode materials. Problems with surface diffusion of silica from the electrolyte were encountered, leading to a blocking of the electrode-electrolyte interface[156].

2.1.8 $LaBaGaO_4$ structured materials

$LaBaGaO_4$ contains gallium in a distorted tetrahedral environment and ordered alternating layers of lanthanum and barium. The gallate tetrahedra are clearly seen to be isolated moieties within the lattice (Figure 16), as reported by Kendrick *et al*[157]. They performed density functional theory (DFT) calculations and found that oxide-ion vacancies were accommodated in the structure through the formation of Ga_2O_7 defects, which are also integral to the mechanism of oxide-ion conduction. The authors describe the oxide-ion conduction mechanism as an unusual cooperative "cog-wheel"-type process involving the breaking and re-formation of Ga_2O_7 units, as well as the relatively facile rotation of the GaO_4 units. Although it presents good oxygen ionic conductivity at high temperatures, experiments in wet atmospheres demonstrate that this system has high proton conductivity ($\approx 1 \times 10^{-4}$ S cm^{-1} at 500 °C) and hence may find application in an alternative device[158].

2.1.9 Melilite structured electrolytes ($LaSrGa_3O_7$)

$LaSrGa_3O_7$ adopts the melilite structure, which consists of alternating cationic $(La/Sr)_2$ and corner-sharing tetrahedral anionic Ga_3O_7 layers and features five-fold tunnels that accommodate the eight-coordinate La/Sr as chains of cations[159]. This composition is an insulator and was found as a secondary phase in the synthesis of the Sr, Mg-doped lanthanum gallate (LSGM) electrolyte[22]. Rozumek *et al.* showed that the La/Sr ratio can be extended to $La_{1.6}Sr_{0.4}$, which presented a conductivity of ~0.1 Scm^{-1} at 950 ^oC and an oxygen transport number of 0.80-0.95 above 600 ^oC[160]. However, Raj *et al.* reported that the La/Sr ratio can only be extended to $La_{1.05}Sr_{0.95}$

without the formation of a Sr-doped $LaGaO_3$ perovskite impurity (LSG), with an oxide ion conductivity of ~10^{-3} Scm^{-1} at 950 ^oC[161].

Recently, Kuang et al. reported the single phase melilite $La_{1.54}Sr_{0.46}Ga_3O_{7.27}$, obtained by reaction at 1200 ^oC for 12h and 1400 ^oC for 12h of a starting material with cation ratios $La_{1.54}Sr_{0.46}Ga_{3.05}$[162]. This material presents a high total conductivity of 0.02 Scm^{-1} at 600 ^oC and 0.1 Scm^{-1} at 900 ^oC. Their structural investigation by neutron powder diffraction shows that the interstititial oxygen located within the A cation tunnels at the level of the gallate sheets is responsible for the high oxide ion conductivity at high temperatures, and the decrease of the activation energy from ~0.85 eV below 400 ^oC to ~0.42 eV over the 600-1000 ^oC temperature range. Whilst of considerable interest this development requires significant further work before being adopted as a viable solid electrolyte.

2.2 Novel Cathodes

2.2.1 Perovskite-type materials

Most of the current cathode materials are based on the perovskite-type ABO_3 structure with one of the conventional materials being LSM ($La_{1-x}Sr_xMnO_3$) as introduced earlier in section 1.3. Other materials currently under development are based on the analogous system $La_{1-x}Sr_xCoO_3$. These are viewed as traditional cathode materials, but through substitution, primarily of the La site several new cathode compositions have been proposed. These are discussed in subsequent sections.

2.2.2 The $Ln_{1-x}Sr_xMnO_3$ system

Introducing A-site substituents into the manganite perovskites has been reported to generate cation vacancies and the effect of this on the ionic and electronic transport

properties of these materials has been widely studied[34, 36]. For example, the electrical conductivity of $Ln_{1-x}A_xMnO_{3\pm\delta}$ at moderate A^{2+} (A = Alkaline earth) concentrations increases with *x* as the Mn^{4+} fraction increases, as described by Tsipis *et al*.[1] Complementing these experimental studies De Souza *et al.*[163] have used atomistic simulation to model the energetics of cation migration and formation in substituted perosvkites. They found that in both rhombohedral and orthorhombic phases oxidative non-stoichiometry leads to cation vacancy formation on *both* cation sites with a tendency for La vacancies to form preferentially. These details are essential in understanding the behaviour of the material in a device and also in understanding the degradation processes that can lead to the formation of insulating phases which affect cathode performance detrimentally, as it is well known that LSM reacts with the YSZ electrolyte forming the insulating pyrochlore phase $La_2Zr_2O_7$. In order to avoid this reaction, Sakaki *et al.* examined the Pr, Nd and Sm analogues[164], as the reactivity with YSZ to form $Ln_2Zr_2O_7$ becomes lower on decreasing Ln^{3+} radius. They analyzed thermal expansion coefficient, reactivity and electrical conductivity data, and determined that the most promising electrode materials were $Pr_{0.7}Sr_{0.3}MnO_3$ and $Nd_{0.7}Sr_{0.3}MnO_3$. An improvement of between 0.5 and 1 order of magnitude in the electrical conductivity was also found by Wen *et al.* for the $Ln_{0.7}Sr_{0.3}MnO_3$ composition (Ln = Pr, Nd, Sm)[165]. The superior properties of praseodymium-containing solid solutions is clearly observed in Figure 17 [1, 166-168], and may be associated with a non-negligible contribution of the $Pr^{3+/4+}$ redox couple at the electrode surface and with a less pronounced interaction with zirconia during cell fabrication and operation. For example, $Pr_{0.7}Ca_{0.3}MnO_3$ showed a maximum conductivity of 266 S cm^{-1} at 1000 ^oC (about 3 times higher than that of LSM) and no evidence of reaction with the electrolyte up to 1200 ^oC[169].

Further improvements in the performance of cathode materials can be achieved by co-doping on both A and B sites. Phillipps *et al.* found that doping with Co on the B

site improved the conductivity of $Gd_{1-x}(Sr,Ca)_xMnO_3$ by up to one order of magnitude in comparison with LSM[170]. Partial substitution on the B sites with Al or other transition metal oxides have also been shown to improve the total conductivity[171, 172].

2.2.3 $Ln_{1-x}A_xFe_{1-y}M_yO_{3-\delta}$ and $Ln_{1-x}A_xCo_{1-y}M_yO_{3-\delta}$ system

Iron-containing oxide phases are stable under SOFC cathodic conditions and exhibit, in general, larger electronic or mixed conductivity than in the LSM system. The highest level of electronic and ionic transport has been found for the $La_{0.5}Sr_{0.5}FeO_{3-\delta}$[173, 174] composition. An important disadvantage of these perovskite ferrites is their high thermal expansion coefficient (TEC) (α values typically between 15 and 25 x 10^{-6} K^{-1}) in comparison with the common solid electrolytes (of about 10-11 x 10^{-6} K^{-1})[175, 176]. Another important issue is the reactivity of the ferrite with the electrolyte material. A significant advantage with the ferrites is that the rate of formation of the zirconate phase ($La_2Zr_2O_7$) is reported to be much lower in comparison with lanthanum manganites, and can be further reduced by incorporation of Al^{3+} [177]. Double substituted materials with a slight A site deficiency were investigated by Kindermann *et al.*[178] showing that the reactivity of $(La_{0.6}Ca_{0.4})_xFe_{0.8}M_{0.2}O_3$ (M= Cr, Mn, Co, Ni) compositions with yttria-stabilized zirconia is minimised when M= Mn, highlighting the complexity of designing a suitable cathode candidate for high temperature operation. For lower temperatures of operation where ceria electrolytes would be used the reactivity with the oxide ferrites is negligible for these compositions. The introduction of doped ceria buffer layers between the cathode and the YSZ electrolyte for high operating temperatures significantly improves the SOFC performance[179].

Perovskite related cobaltites present considerably better cathodic and transport properties that the analogous manganites and ferrites, however they also present higher thermal and chemical expansion[180, 181]. Initially, of most interest was the $La_{1-x}Sr_xCoO_{3-\delta}$(LSC) composition, possessing significant oxide ion conductivity and high

electronic conductivity[182]. In considering the use of cobaltite cathodes the choice of the electrolyte is of importance. LSC was found to react with zirconia but presents superior performance when tested with $Ce_{0.8}Sm_{0.2}O_{1.9}$ (SDC) and $Ce_{0.8}Gd_{0.2}O_{1.9}$ (GDC)[183].

Adler[184] has investigated the behaviour of LSC porous electrodes by AC impedance spectroscopy and has found that the oxygen reduction reaction is limited by surface chemical exchange and solid state diffusion, contrary to the commonly accepted view that the electrode reactions are charge transfer limited. Furthermore he has also found that the reduction reaction extends over several microns and under certain conditions may approach the thickness of the electrode. Isotope exchange measurements on dense LSC deposited on a $Ce_{0.9}Ca_{0.1}O_{1.9}$ electrolyte were performed by Kawada *et al.*[185]. These experiments showed that the isotope exchange rate was controlled by the surface exchange process, supporting the findings of Adler. van Doorn *et al.* [186] have also focused on the effect of structure on the ionic conductivity. A variety of compositions ($0<x<0.8$) were studied and they have found evidence for the existence of oxygen vacancy ordering in these materials where $x>0.5$. At this composition LSC adopts a cubic structure, whereas at $x<0.5$ it is rhombohedral. High resolution TEM (HRTEM) and selected area electron diffraction (SAED) measurements at the x= 0.7 composition confirmed the presence of superstructure ordering, where it was proposed that the ionic conductivity would be lower than in disordered regions.

Replacement of lanthanum with Gd, Sm or Dy in LSC has been investigated in an attempt to produce materials of greater chemical stability, but it was established that at temperatures of greater than 900 ^{o}C $SrZrO_3$ phases formed, and therefore these materials are only attractive candidates for low temperature SOFC applications[170, 187, 188].

To overcome the technological problems associated with the LSC materials at high temperatures, B-site substitutions have been developed. One interesting example refers to the $La_{1-x}Sr_xCo_{1-y}Fe_yO_3$ (LSCF) composition, initially studied by Tai *et al.*[189] In this work they identified the rhombohedral/orthorhombic transition at *y*=0.8 for the *x*=0.2 composition and also studied the effect this had on thermal expansion. Details of TECs and total conductivity values for different compositions can be found in Table 3. As can be seen in the table, moderate dopant additions provide a significant enhancement in the total conductivity and electrochemical activity, but also increase apparent TECs. Kostogloudis *et al.*[190] reported that, on the creation of La-site cation vacancies, the conductivity and thermal expansion both decrease owing to the dominant charge compensation mechanism via oxygen vacancy formation. The charge compensation mechanism in these A-site deficient perovskites is then the formation of oxygen vacancies, rather that the oxidation of Mn^{3+} to Mn^{4+} as for LSM.

Tu *et al.*[191] have also studied a series of LSCF materials varying the type of lanthanide ion. They found that all compositions had a high electrical conductivity with $Nd_{0.6}Sr_{0.4}Co_{0.8}Fe_{0.2}O_{3-\delta}$ having the highest conductivity (~600 S cm^{-1} at 400 ^oC), and catalytic activity for oxygen reduction.

2.2.4 Ruddlesden-Popper type compounds

Ruddlesden-Popper type materials have the general formula $A_{n+1}M_nO_{3n+1}$, and adopt the structures observed in the $Sr_{n+1}Ti_nO_{3n+1}$ titanates, first reported by Ruddlesden and Popper[192]. The structure of the Ruddlesden-Popper phases consists of n consecutive perovskite layers $(AMO_3)_n$ alternating with rock salt layers (AO), with AO along the crystallographic *c* direction. The well-known perovskite AMO_3 and K_2NiF_4-type (A_2MO_4) structures correspond to n = ∞ and n = 1 respectively, Figure 18. Ruddlesden-Popper phases present attractive electrochemical and transport properties, but chemical phase stability in the range of temperatures and oxygen

chemical potentials necessary for the SOFC applications is still an issue[193-195]. Several K_2NiF_4-type compounds have been proposed as SOFC cathodes, including those with A = La, Sr, Ba, Pr, Nd and M = Ni, Cu, Co, Fe[196-199]. The total conductivity of K_2NiF_4-type nickelates remains predominantly *p*-type electronic in the entire $p(O_2)$ range. For these compounds, the bulk ionic transport occurs via anisotropic diffusion of interstitial ions in the rock-salt-type layers and vacancies in the perovskite layers[198]. Oxygen permeation through the dense material is reported to be limited by the surface exchange rate[199]. The hole transport is lower than that in the perovskite analogues, but still sufficient for practical applications. Small amounts of A^{2+} doping leads to a higher conductivity and lower oxygen content, with a negative impact on the oxygen diffusivity, which is determined by the interstitial anion migration[200]. Evidence for the diffusion path of oxide ions in a K_2NiF_4-type mixed conductor was firstly reported by Yashima *et al.*[201] for the $(Pr_{0.9}La_{0.1})_2(Ni_{0.74}Cu_{0.21}Ga_{0.05})O_{4+\delta}$ compound through a high-temperature neutron powder diffraction study. The nuclear-density distribution shows the two-dimensional (2D) network of the O2-O3-O2 diffusion paths of oxide ions where O2 represents the oxygen at a (0, 0, *z*) position, and O3 represents the interstitial oxygen located at a 16*n* site (see Figure 19). This result is also consistent with the anisotropic transport of oxide ions in $La_2NiO_{4+\delta}$[202, 203].

Figure 20 presents the electrochemical behaviour of different nickelate-based electrodes and it is clear that for the $Ln_2NiO_{4+\delta}$ (Ln = La, Nd, Pr) series, relatively low polarization resistances were observed[126]. The high performance of the Pr analogue may be a result of the metastability of the praseodymium nickelate, which decomposes into PrO_x and $Pr_4Ni_3O_{10-\delta}$, having higher ionic and electronic conductivities[194]. Kim *et al.*[204] performed AC impedance measurements and suggested that the electrode reaction is limited by the surface exchange reaction for the $La_2NiO_{4+\delta}$ These results are in agreement with the enhancement of the

electrochemical activity of $La_2Ni_{0.8}Cu_{0.2}O_{4+\delta}$[205] and $LaNi_{0.5}Fe_{0.5}O_{3-\delta}$[206] by surface modification with praseodymium oxide.

Much of the work on these materials has focused on the chemical and electrical characterization. Compatibility of these materials with the electrolyte is also an important issue to be addressed. For this purpose, Munnings *et al.* [207] reported on the stability and reactivity of the $La_2NiO_{4+\delta}$ with the LSGM electrolyte. They found an effect on the surface stoichiometry and that this stoichiometry change adversely affected the cathode performance. They also observed that the best performance of the $La_2NiO_{4+\delta}$ cathode was on surfaces with elevated levels of strontium and magnesium. Thermodynamic modelling calculations made by Solak *et al.*[208] also show that $La_2NiO_{4+\delta}$ is not chemically compatible with the LSGM electrolyte not only at fabrication conditions but also at operation conditions. On the contrary, Sayers *et al.*[195] recently found that there is no evidence of secondary phase formation on $La_2NiO_{4+\delta}$-LSGM mixtures from the obtained diffraction data over a period of 72h at temperatures of up to 1000 ^oC. They also found that there is significant reactivity between $La_2NiO_{4+\delta}$ and CGO after 24h at 900 ^oC, with the formation of a higher order Ruddlesden-Popper ($La_{n+1}Ni_nO_{3n+1}$) phase as one of the reaction products.

Another interesting material presenting the K_2NiF_4-type structure is $Sr_{2-x}La_xMnO_{4+\delta}$. Munnings *et al.*[209] reported that this material presents similar TEC to the most common electrolyte materials and is also chemically stable over a wide range of oxygen partial pressures. Liping *et al.* recently studied the reactivity between $Sr_{1.4}La_{0.6}MnO_{4+\delta}$ and a CGO electrolyte and no reaction was found after heat treatment at 1000 ^oC for 12 hours[210]. However these materials have been shown to have relatively low electronic conductivities of the order of 2 Scm^{-1} and are therefore unlikely to be used as cathodes.

2.2.5 Barium Strontium Cobalt Ferrite (BSCF)

$Ba_{0.5}Sr_{0.5}Co_{0.8}Fe_{0.2}O_{3-\delta}$ is a cubic perovskite material in the $BaCoO_{3-\delta}$-$SrCoO_{3-\delta}$ system, which was firstly developed for high-temperature oxygen permeation membrane applications[211]. Shao *et al.*[42] firstly proposed this material for intermediate temperature fuel cell applications and reported high power densities of about 1 W cm^{-2} at 600 ^oC and 0.4 W cm^{-2} at 500 ^oC on a BSCF-SDC-Ni/SDC cell when operated with humidified hydrogen and air, in the anode and cathode side respectively. Wang *et al.*[212] calculated the TEC for the $Ba_{0.5}Sr_{0.5}Co_{0.8}Fe_{0.2}O_{3-\delta}$ composition from high temperature XRD data and they obtained a value of 11.5×10^{-6} K^{-1}, which is comparable with most of the electrolytes used in SOFCs. Higher values for the TEC (~$20x10^{-6}$ K^{-1}) were obtained from neutron diffraction data by McIntosh *et al.* for the same composition[213], and also measured by Zhu *et al*. (19.2-22.9 x 10^{-6} K^{-1})[214]. In this work they also reported on the chemical compatibility of BSCF with 8YSZ and 20GDC. They found no reaction up to 800 ^oC but above 800 ^oC severe reactions were detected. In terms of chemical compatibility, similar results were also obtained by Duan *et al.*[49] BSCF cathodes have, however, also been tested with LSGM as the electrolyte with no apparent reaction between phases[215]. Nevertheless best results were found when using the BSCF cathode with GDC as the electrolyte. For example, Liu *et al.* obtained ~1300 mW cm^{-2} at 600 ºC on a BSCF-GDC-Ni/GDC cell[216].

Li *et al.* showed by AC impedance spectroscopy that Nd-doped BSCF presents higher electrical conductivity than BSCF. It also presents better electrochemical performance than the BSCF cathode, probably determined by a combination of the high electrical conductivity and the amount of oxide ion vacancies in the cathode[217].

2.2.6 Cerium niobate

Cerium niobate ($CeNbO_{4+\delta}$) is of interest for SOFC applications due to its wide range of oxygen stoichiometries, varying from $CeNbO_4$ to $CeNbO_{4.33}$[218]. It also presents a

large open structure, which is potentially beneficial for fast oxide ion conduction. The crystal structure of this material at room temperature is monoclinic fergusonite (*I*2/*a*), and on heating exhibits a phase transition at approximately 1023 K in air to a tetragonal scheelite ($I4_1/a$)[219]. The scheelite material exhibits a reasonably high total conductivity (0.030 S cm^{-1} at 850 ^oC) and also presents mixed ionic/p-type electronic conduction (ionic transference number = 0.4)[220], due to the mixed valence of Ce and interstitial oxygen anions. In this work, it was found that the high temperature scheelite polymorph is unstable at low partial oxygen pressures. Packer *et al*.[221] have studied the oxide ion diffusion in cerium niobate and found a relatively high value for D^* = 8.29 x 10^{-8} cm^2 s^{-1} at 850 ^oC and a good surface exchange coefficient (k^* = 6.85 x 10^{-7} cm s^{-1} at 850 ^oC). Despite its high oxide ion diffusion, the electronic conductivity is currently too low for SOFC cathode applications. More work is therefore required in order to improve this aspect of the material, but improvements could be achieved through the use of composites (with an electronic component) and also via substitution on the Ce site[222], with for instance La, or on the Nb site[223] with vanadium. The full range of possible substitutions is extensive and should be carefully considered to optimise all aspects of cathode performance.

Recent studies by in-situ X-ray powder diffraction revealed that $CeNbO_4$ decomposed to CeO_2 and $CeNb_3O_9$[224] under a pure oxygen atmosphere. The decomposition temperature is shown to decrease with decreasing partial pressure of oxygen, and decomposition of $CeNbO_{4+\delta}$ at lower partial pressures of oxygen is kinetically hindered, as it can be seen in Figure 21.

2.2.7 Double perovskites, $A_2B_2O_{6-\delta}$

$GdBaCo_2O_{5+\delta}$ (GBCO) adopts the double perovskite structure with orthorhombic symmetry, in which Co ions are coordinated in square pyramids (CoO_5) and octahedra (CoO_6), which alternate along the *b*-axis[225]. The Ba cations are ordered in

alternating (001) layers with oxygen vacancies mainly located along (100), in the $[GdO]_x$ planes (see Figure 22)[226]. This material was reported to have rapid oxygen transport kinetics at low temperatures[227], and was firstly proposed for IT-SOFC cathode applications by Chang *et al.*[228] They found by AC impedance spectroscopy that GBCO cathode materials exhibit good performance at low temperatures on CGO electrolytes. Furthermore, high oxygen surface exchange ($k^* = 2.8 \times 10^{-7}$ cm s^{-1}) and reasonable oxide ionic diffusivity ($D^* = 4.8 \times 10^{-10}$ cm^2 s^{-1}) were obtained for GBCO at 575 ^oC[229]. These authors also reported an area specific resistance of 0.25 Ωcm^2 at 625 ^oC for a GBCO/CGO/GBCO cell. Similar results were obtained by Li *et al.* [230] for the GBCO cathode on the SDC electrolyte. Peña-Martínez *et al.*[231] also reported no reactivity and good electrochemical performance of the GBCO cathode with the LSGM electrolyte, indicating that this is one of the most exciting alternatives to the ABO_3 cathodes discussed earlier.

The effect of Sr substitution for Ba in the GBCO material on the structural chemistry has been investigated[232]. The $GdBa_{1-x}Sr_xCo_2O_{5+\delta}$ system exhibits a structural change from an orthorhombic *Pmmm* (x = 0) to tetragonal *P4/mmm* (x = 0.2-0.6) to a further orthorhombic *Pnma* (x = 1) structure. The x = 0.2 and 0.6 samples exhibit higher power density when tested as an SOFC cathode than either the x = 0 and x = 1 samples, partly due to faster oxygen transport within the tetragonal structure. While the parent $GdBaCo_2O_{5+\delta}$ sample suffers from interfacial reaction with LSGM and CGO electrolytes at 1100 °C, Sr substitution for Ba greatly improves the chemical stability of $GdBa_{1-x}Sr_xCo_2O_{5+\delta}$.

The analogous material $PrBaCo_2O_{5+\delta}$ (PBCO) has also been suggested as a SOFC cathode due to its unusually rapid oxygen transport kinetics at low temperatures (300–500 °C)[233, 234]. Zhu *et al.*[235] demonstrated the suitability of PBCO for IT-SOFC applications. They preformed electrochemical measurements on a PBCG/SDC/Ni-

SDC single cell obtaining a maximum power density of about 850 mW cm^{-2} at 650 ^{o}C. Moreover, the samarium derivative ($SmBaCo_2O_{5+\delta}$) presents good electrochemical properties and has also been recently proposed as a cathode material for IT-SOFC[236].

2.2.8 Mixed conducting composites

The use of composite cathodes generally includes an electronically conducting material and a solid electrolyte. By the introduction of the solid electrolyte, the electrochemical reaction zone is enlarged, and the microstructural stability and adherence to the electrolyte is therefore also enhanced. The incorporation of crystalline nanocatalysts onto the cathode could also improve the performance of the electrodes[237-239].

The most studied composite cathode to date is LSM/YSZ[240-243]. The connectivity of the electronically conducting LSM and ionically conducting YSZ phases is crucial to produce a mixed conducting composite, because the ionic conductivity of LSM and the electronic conductivity of YSZ are negligible under normal SOFC operating conditions. Results from electrochemical measurements performed by Haanappel *et al.*[244] showed the highest performance when using an LSM/YSZ mass ratio of 50/50. Recently, Princivalle and Djurado reported on the fabrication of LSM/YSZ composite films prepared by electrostatic spray deposition (ESD) with various compositions and microstructures[245]. By this technique they prepared LSM/YSZ composites with simultaneous graded composition and porosity adjusting the YSZ content and nozzle-to-substrate distance at a constant substrate temperature. Electrical and electrochemical properties of these promising composites are still unknown. Huang *et al.* also reported an improvement on the performance of LSM-based cathodes through doping with Co-containing compounds, forming the $La_{0.8}Sr_{0.2}Mn_{0.75}Co_{0.25}O_3$/YSZ composite[246].

Composites of LSM with other electrolyte materials such as scandia stabilised zirconia (ScSZ)[247, 248], CGO[249], $Ce_{0.7}Bi_{0.3}O_2$ (CBO)[250] or yttria-stabilized bismuth oxide (YSB)[251] have also been shown to improve the cathode performance. Another interesting manganite based composite is the $La_{0.8}Sr_{0.2}Sc_{0.1}Mn_{0.9}O_{3-\delta}$-ScSZ. Using a mass ratio of 80/20, Zheng *et al.*[252] showed high power densities of about 1200 mW cm^{-2} at 800 ^oC on an anode supported Ni-ScSZ/ScSZ/$La_{0.8}Sr_{0.2}Sc_{0.1}Mn_{0.9}O_{3-\delta}$-ScSZ cell.

Mixed ionic and electronic conductors (MIEC) used in combination with the electrolyte material (usually SDC or GDC) to form a composite also present superior performance in comparison with the pure MIEC, as shown, for example, in the $Sm_{0.5}Sr_{0.5}CoO_3$-$Sm_{0.2}Ce_{0.8}O_{1.9}$ (75/25 wt. %)[253], $SrCo_{0.8}Fe_{0.2}O_{3-\delta}$-$La_{0.45}Ce_{0.55}O_{2-\delta}$ (50/50 wt. %)[254], $LaNi_{0.6}Fe_{0.4}O_3$-SDC (50/50 wt. %)[255], and $Pr_{0.7}Sr_{0.3}Co_{0.9}Cu_{0.1}O_{3-\delta}$-SDC (65/35 wt. %)[256] composites. Adding an ionic conducting phase to the LSCF electrode also reduces the cathode polarisation, as reported for LSCF-GDC and LSCF-SDC[257-260], LSCF-LSGM[261] and LSCF-YSZ[262] composites.

Camaratta *et al.*[263] recently reported on the $Bi_2Ru_2O_7$–$Bi_{1.6}Er_{0.4}O_3$ composite applying pure $Bi_2Ru_2O_7$, a pyrochlore oxide, as a current collector to the electrode surfaces. The lowest value of ASR they obtained was 0.73 Ω cm^2 at 500°C and 0.03 Ω cm^2 at 700°C, one of the lowest SOFC electrode ASR values reported to date, making this composite a good candidate for IT-SOFCs.

Concerning the Ruddlesden-Popper series, Laberty *et al.*[264] reported on the performance of solid oxide fuel cell cathodes with lanthanum-nickelate-based composites. They showed that lanthanum nickelate performs poorly when used as a single-phase cathode in yttria-stabilized-zirconia-based air-H_2 button cells at 800 °C. However high power densities of up to 2.2 W cm^{-2} were measured using a $La_2NiO_{4+\delta}$-SDC composite bilayer cathode.

BSCF composites, such as BSCF-$LaCoO_3$[265], BSCF-SDC[266] and BSCF-$Sm_{0.5}Sr_{0.5}CoO_{3-\delta}$[267] have also been proposed as good IT-SOFC cathodes. For example, the BSCF-$LaCoO_3$ composite presents an ASR as low as 0.21 Ω cm^2 at 600 ºC for the 30 vol% of LSC-BSCF.[265]

2.3 Ceramic and sulphur tolerant anodes

As discussed earlier in section 1.2, conventional cermet anodes suffer from issues of redox stability, coking and sulphur poisoning. In an effort to develop high durability anodes that overcome these limitations the modification of typical cermet materials to offer greater resistance to coking and sulphur poisoning has been considered. Elsewhere novel ceramic anodes have been proposed to achieve the same objective. Each of these potential materials solutions are attractive and will be addressed in turn.

2.3.1 Redox tolerant cermets

A number of approaches have been adopted to modify the current Ni-based cermets including substitution of Ni with alternative metals. Replacement of Ni with Cu has been reported to reduce the affinity of Ni for hydrocarbon cracking that leads to coking of the anode. In developing Cu cermets many strategies have demonstrated successful anode performance. Park and co-workers pioneered the use of Cu based cermets demonstrating that SOFCs can operate effectively with a Cu-ceria cermet, where the ceria acts as a catalyst for the oxidation of hydrocarbons and Cu is used as it is an excellent electronic conductor[268, 269]. Synthesis of the cermets has generally focussed on the use of impregnation methods to infiltrate the Cu phase into the YSZ parent phase. Jung et al have investigated the use of both aqueous $Cu(NO_3)$ and aqueous $Cu(NO_3)$/urea[270] to introduce Cu and have studied the effect of

the starting solution on the particle morphology and ultimately fuel cell performance. A typical micrograph illustrating the distribution of Cu achieved is shown in Figure 23.

Cu is a poor catalyst with respect to the C-H bond and hence overcomes the issues of carbon deposition, allowing methane and alternative higher hydrocarbons to be used as the fuel. This is illustrated by the direct comparison of the performance of anodes both with and without the ceria content, Figure 24, as detailed by He *et al.*[271] Indeed Gorte *et al*. demonstrated that a cell with a Cu-ceria anode operating on n-butane, toluene, methane, ethane and 1-butene had reasonable power densities of 0.12 W cm^{-2} at 973K[269]. However, the power densities obtained are relatively modest, as acknowledged by the authors, and compare unfavourably with cells using H_2 as a fuel (0.3 W cm^{-2})[269] and to those cells operating with Ni-YSZ anodes on H_2 at 800 ^oC (1.0 W cm^{-2})[272]. These comparisons are perhaps somewhat unfair as the Ni-YSZ based cells have undergone decades of materials, composition and microstructural optimisation that could conceivably enhance the performance of the Cu based system proposed. As illustration of this Costa-Nunes *et al.*[273] developed a Cu-CeO_2-YSZ anode systems using CO as a fuel that achieved higher performance than with H_2 fuel, achieving up to 370 $mWcm^{-2}$. A further development has been demonstrated by Ye *et al.*[274] where a Cu-CeO_2-ScSZ cermet was tested with H_2 and C_2H_5OH/H_2O environments, but poor performance resulted at all temperatures, achieving a maximum power density of 372$mWcm^{-2}$ at 800^oC and only 130 $mWcm^{-2}$ at 700^oC.

To illustrate the effect of Cu content on carbon formation a series of Cu-Ni alloys were incorporated into YSZ based anodes and significant suppression of coking achieved. It was also noted that the use of alloys is a relatively unexplored domain and of interest as the catalytic activity of the alloy is not directly related to the properties of the parent metals, and hence the alloy activity is not simply a summation of the two metals individual properties[275].

Of course the use of Cu based cermets raises the issue of both chemical and thermal compatibility between components used in the cermet and recent work has indicated that YSZ and CuO will react, producing a monoclinic ZrO_2 phase[276]. Whilst CuO is not used in the anode itself many manufacturing processes are initiated with the metal oxide and subsequently reduced. Starving the fuel cell of fuel during thermal excursions could also cause oxidation of the anode and hence reactivity of the oxides is significant. Although Ruiz-Morales *et al.*[276] report reactivity they also indicated that the formation of monoclinic ZrO_2 did not adversely affect the polarisation resistance of the cell which was attributed to the compensation of the low conductivity of the ZrO_2 phase by the high electronic conduction of Cu.

Further studies have been undertaken to characterise the potential of cermets based upon Cu-SDC[270, 277-282]. In most cases it was found that additional CeO_2 had to be incorporated into the composition as SDC is a relatively poor catalyst for hydrocarbon oxidation. There was speculation that despite Cu having no hydrocarbon oxidation activity, the catalysis of water gas shift reactions by Cu could have a beneficial effect and hence a comparison of Cu-SDC-CeO_2 and Au-SDC-CeO_2 was performed. Measurements in gas atmospheres of H_2 and n-butane at 650^oC, showed no significant difference in performance, indicating that Cu serves as a purely electronic conductor in these cermets[279] and that CeO_2 adopts a critical catalytic role in hydrocarbon oxidation.

Further modification of the composition of cermets by introducing LSGM to the CeO_2:Cu ratio was also investigated with the intention of using these anodes at intermediate temperatures. Three ratios of Cu:Ni in LSGM were studied (0.7:0.3, 0.5:0.5, 0.3:0.7) with the conclusion being that LSGM showed good stability towards the metallic components at temperatures below 1000^oC, however the poor catalytic activity of the Cu negated the use of these materials[283]. A proposal to introduce CeO_2 to this composition was considered to enhance the catalysis. In this case

however only H_2 gas was considered and no hydrocarbon content included in the fuel feed. In contrast, An *et al.*[284] achieved a far superior performance on a thick (440μm) LSGM electrolyte with a Cu-CeO_2-LSGM anode in both H_2 and C_4H_{10} fuels, attaining a maximum power density of 220mWcm^{-2} at 700^{o}C. Analysis of the electrode data obtained from these cells suggested that the anode was limiting the cell performance as 2/3 of the cell polarisation resistance could be attributed to the anode.

Of course there is no reason to restrict the cermet to a single metal type and efforts have been expended to introduce Fe and Co to the Ni-YSZ cermet[285]. Through the use of a combustion synthesis technique it has been shown that nanometric scale powders with high surface areas, essential for catalytic activity, can be easily produced. In this work the Ni-Fe composition was determined to have the highest surface area by BET, with 33 m^2g^{-1}. Whilst Ni and Cu cermets are the most prevalent there has also been some interest in Co-YSZ cermets[286] with comparison of the effect of synthesis conditions on the overall performance of the three types of anode. Significant differences in the impedance spectra of the three anodes was observed, Table 4, which the authors ascribe to differences in the particle size ratio between the YSZ phase and the metal. In each case three components were identified which are attributed to high, medium and low frequency responses corresponding to charge transfer, dual phase boundaries and mass transport respectively.

One further materials solution that has been proposed is the use of substituted YSZ in the cermet. Commonly the use of Ti as a substituent has been attempted[287, 288], with a typical composition being $Y_{0.2}Ti_{0.18}Zr_{0.62}O_{1.9}$ (YZT) combined with CuO. These cermets were shown to have the requisite high electronic conductivity, but unfortunately they underwent Cu segregation at temperature leading to a degradation of the microstructure of the electrode. However, electrochemically they were identified as favouring hydrogen oxidation reactions rather than H_2 evolution, making

these materials good candidates for SOFCs. In this work, however poor electrode microstructure led to relatively poor performance. Further optimisation of the YZT concept was achieved through the further substitution of Ce giving $Y_{0.15}Zr_{0.57}Ti_{0.13}Ce_{0.15}O_{1.925}$ which was then tested with both NiO and CuO as cermets[288]. The best performance was identified for the YSTC sample with 60% CuO at 500 ^{o}C, with conductivity 5 times higher than that for the corresponding NiO cermet. Again, it was found that degradation of the microstructure occurred with the copper based cermets on increasing temperature, and hence is a concern when considering the Cu based cermets for SOFCs. These authors also found that performance of all of the composites tested was inferior to the Ni-YSZ standard and conclude that this may be due to the microstructure, again indicating the difficulty of designing a functional anode that competes with or improves upon Ni-YSZ.

2.3.2 Ceramic anodes

Perhaps a logical step in the evolution of anode materials is the development of single phase ceramic or oxide anodes. Evidently this solution presents some significant materials challenges, perhaps mostly concerned with stability at low pO_2, but offers the potential of sulphur tolerance and thus higher durability. Given the large array of possible oxides that could be tested as anodes it is perhaps unsurprising that efforts were directed towards familiar structural chemistries, and hence early studies have considered perovskite-type anodes[289-291], with excursions to tungsten bronzes[292, 293] and double perovskites[294]. Relatively few studies of the tungsten bronze type, $A_{0.6}BO_3$ compositions have been undertaken, with the best performance found to be with the $Sr_{0.2}Ba_{0.4}Ti_{0.2}Nb_{0.8}O_3$ material that achieved a conductivity of 10 Scm^{-1} at 10^{-20} atm[292, 293]. Despite this, overall cell performance was found to be inferior to current standard materials and hence further work has not been forthcoming with this class of materials. $Sr_2Mg_{1-x}Mn_xMoO_{6-\delta}$, a double perovskite, was developed to extend the lifetime of anodes and findings confirmed that if only the

Sr_2MgMoO_6 composition was employed sulphur tolerance was much improved, indicating the negative effect of Mn in this case. However, despite this initial promise no further advances in double perovskite anodes have been presented.

One of the earliest reports of a novel perovskite oxide anode was concerned with the use of $La_{0.6}Sr_{0.4}Co_{0.2}Fe_{0.8}O_{3-\delta}$[295] as an anode rather than a cathode with the intention being to directly oxidise methane at the anode. These authors investigated the stability of LSCF in anodic conditions consisting of temperature programmed reaction of 3% CH_4 in 6% O_2 with an unspecified balance gas. From these measurements it was evident that the catalyst was active for methane decomposition but that there were concerns over the stability of the composition at elevated temperatures for timescales applicable to devices. Further developments have subsequently focussed on the use of Mn and Cr based lanthanide perovskites with the aim being to stabilise the material at low pO_2 and high temperature.

Several authors have investigated the substitution of $La_{1-x}Sr_xCrO_{3-\delta}$, using Mn[289, 290], Ru[296] Ni[297] and Fe[298, 299] with studies of the Fe substituted chromates amongst the earliest ceramic anode studies. Ramos and Atkinson[298] investigated the oxygen transport characteristics of the $La_{1-x}Sr_xCr_{1-y}Fe_yO_{3-\delta}$ material where x = 0.2, 0.4 and 0.6 under both oxidising and reducing conditions, finding that significant oxygen transport was present under a $H_2/N_2/H_2O$ atmosphere. Indeed these authors find that under oxidising conditions at a temperature of 800^oC oxygen diffusion coefficients (D*) of the order of $10^{-8}cm^2s^{-1}$ were obtained for materials where x = 0.4, whilst somewhat surprisingly under reducing conditions the diffusion coefficient at 800^oC was of the order of $10^{-7}cm^2s^{-1}$. A further increase in D* on proceeding from x = 0.2 to x = 0.4 of 2 orders of magnitude was also observed. Whilst these data are encouraging there remain concerns over this material regarding its redox stability.

To overcome these concerns the majority of subsequent studies focussed on the use of Mn substitution in the chromate lattice. Tao *et al.*[289] for example developed the $La_{0.75}Sr_{0.25}Cr_{0.5}Mn_{0.5}O_{3-d}$ (LSCM) composition investigating the structural chemistry and redox stability, finally investigating the performance of the material as an anode in a single fuel cell. Through a variety of testing conditions including atmospheres containing CH_4, 5% H_2 and/or 3%H_2O the optimum performance was achieved at a temperature of 900^oC giving a power density of 0.5 Wcm^{-2} in a wet H_2 gas stream. Tao claims this gives an anode that is comparable in performance with Ni-YSZ, with the additional benefit of activity towards oxidation of methane in dry atmospheres. Further work has indicated that improved performance can be achieved in these materials with A-site cation deficiency and led to the work of Raj *et al* where oxygen transport data was obtained[300] for the $(La_{0.75}Sr_{0.25})_{0.95}Cr_{0.5}Mn_{0.5}O_{3-d}$ material. In this case, as was observed earlier with similar studies of the ferrites, diffusion coefficients were found to be significantly higher under a reducing atmosphere than in dry O_2. Of concern however was the behaviour of the surface exchange coefficients as a function of temperature in that non-Arrhenius behaviour was observed, which may indicate an increasing concentration of oxygen vacancies on increasing temperature is involved with the charge transfer at the surface of these oxides.

Evidently the requirement for novel redox and sulphur tolerant anodes requires understanding of the electronic conduction properties of materials as well as the ionic conductivity. In LSCM the dependence of electronic conductivity on composition and pO_2 has been detailed and related to the defect chemistry of the bulk oxide[301]. Here the authors used X-ray absorption spectroscopy to probe the cation valence and determined that the defect chemistry was controlled by Mn on the B site and there was no influence on the conductivity exhibited by the Cr on the B-site, as is illustrated in Figure 25. Indeed the authors also suggest that the conductivity exhibited by this material can be attributed to the charge carriers associated with the concentration of

Mn^{4+}, such that defects are generated and compensated electronically on the introduction Sr. The origin of the Mn^{4+} is assumed to be from the disproportionation of Mn^{3+}.

Whilst LSCM has shown some promise as an anode alternative further materials developments have considered the adoption of composites containing this novel material. An initial attempt to improve anode performance involved the creation of a composite of LSCM with Cu[302]. In this work a cell performance of 250mWcm^{-2} was achieved for an anode functioning on an LSGM electrolyte operating at 850^{o}C. Further development was considered by Ye *et al.*[274] who looked at a complex composite combining the LSCM with both an electrolyte component (ScSZ) and a metallic component, Cu. Evaluation of the performance of this anode layer indicated poor electrochemical performance, achieving only 140 mWcm^{-2}, lower than that obtained from a LSCM-Cu anode[302]. To overcome this deficiency in performance a layer of LSCM/Cu/YSZ was deposited on the anode and a significant increase in power density, to 584 mWcm^{-2}, was observed, however the value of this composite anode is questionable given the multicomponent nature of the anode with a total of six components including two different electrolyte materials.

Little further investigation of the LSCM system has been reported and work on perovskite type anodes appears to be directed towards the novel titanate type composition, $La_4Sr_8Ti_{11}Mn_{0.5}Ga_{0.5}O_{37.5-d}$[303, 304] (LSTGM). Initial interest in this composition stemmed from the desire to investigate La substituted $SrTiO_3$ as a potential redox stable anode. In this case the material was further substituted with Ga and Mn and as a result extended point defects were formed, particularly disordered oxygen defects. Disorder was identified in these complex perovskites through the use of high resolution TEM[305], and subsequent testing of the composition as an anode indicated performance comparable to Ni-YSZ with an LSM cathode on YSZ electrolyte[303, 305]. Later improvements in performance were achieved through the use

of composites of LSTGM with Cu[303], leading to lower polarisation resistances, indicating that Cu impregnation of anodes is a likely route to enhanced performance in all anode materials.

Further oxide materials have been prepared and evaluated as potential anode materials, including Nb_2TiO_7[306] and $Gd_2Ti(Mo,Mn)O_7$[307, 308] but have proved to be either extremely redox intolerant or possess very low ionic conductivities. Hence the most promising materials for oxide anodes remain materials structurally related to the ABO_3 perovskite.

3.0 Materials developments through processing

As will be clear from the preceding discussion of materials developments for SOFCs many of the advances in performance of the individual components can be considered to be incremental in nature, with fractional improvements in redox stability, sulphur tolerance, ionic conductivity or thermomechanical stability. It is highly unusual for step changes in performance to be identified, but there have been recent reports and discussions surrounding the potential for nanostructured materials, particularly heterostructured composites, to massively enhance conduction properties within electrolyte layers. Garcia-Barriocanal and co-workers[309] produced a layered YSZ based on $SrTiO_3$ (YSZ/STO) substrates and report an eightfold increase in ionic conductivity, suggesting that devices based on YSZ could operate at close to room temperature, revolutionising SOFC technology. To achieve such significant increases, the authors suggest that the strain at the YSZ/STO interface is critical and allows facile oxygen diffusion pathways to open along this nanostructured interface. Of course these findings are the subject of scepticism as alternative models such as the incorporation of electronic conductivity would also explain these results. However it is suggested that appropriate measurements were carefully performed to

eliminate this possibility, but until reproducible data are collected this advance is likely to be contested. A similar effect has been indentified, but to a lesser degree in heterostructured YSZ[310], where the magnitude of the conductivity has been increased as a function of the number of layers of the electrolyte. Again these data were obtained from conductivity measurements and hence there is no direct measure of the ionic mobility within these structures, however these two sets of data, albeit from different materials and structures, indicate that a nanostructured layer will enhance SOFC performance. Will these effects be maintained over the lifetime of the device is an open question and, once the effects are fully explained, no doubt there will be increased interest in this field.

Closely related to these advances are the possibilities of exploiting anisotropic materials, such as the Ruddlesden-Popper structured materials detailed earlier. As the ionic mobility in these cathode materials is highly *ab* plane dependent, there is an inherent advantage to depositing high quality epitaxial thin films. Indeed preliminary data has been obtained from both single materials such as $La_2NiO_{4+\delta}$[203], and also from single cell devices[311] illustrating the potential of these new materials. Deposition of epitaxial films, using either chemical vapour or pulsed laser deposition techniques, results in highly ordered films oriented closely to a substrate material, either $NdGaO_3$ or STO. This clearly raises the question of the effect of strain on the transport at the electrode/substrate interface and to date no significant enhancement has been determined, somewhat contradicting the studies on YSZ/STO films. These are complex systems and perhaps should not be directly compared, but it is clear that much further work is required to elucidate the details of interfacial transport, including use of modelling techniques.

4.0 Proton conducting ceramic fuel cells

Much of the preceding discussion has concerned the development of solid oxide fuel cells based on oxide ion conducting ceramics. In these devices the electrolyte, cathode and anode all possess significant levels of oxygen ionic conduction and materials selection is then a compromise between the demands of each functional layer. As an alternative proton conducting ceramics have been suggested as the basis for a lower temperature solid oxide fuel cell. In this instance protons are incorporated into the oxide via the following reaction:

$$H_2O(g) + V_O^{\bullet\bullet} + O_O^x \leftrightarrow 2OH_O^{\bullet} \qquad (4.1)$$

where oxygen vacancies combine with H_2O to produce OH^- defects in the lattice. This process consists of many potential steps, but generally results in materials with significant proton conduction at temperatures below about 600^oC. As the temperature increases it is normally the case that oxide ion conduction increases and dominates, restricting the operating regime of ceramic proton conductors to relatively low temperatures. Clearly this could be considered an advantage in the search for new devices.

Proton conducting ceramics are commonly based upon the perovskite structure type with the cerate and zirconate types being most prevalent. Initial studies focussed on the $SrCeO_3$ and $SrZrO_3$ based materials. Uchida et al demonstrated sizeable proton conductivity in each of these materials[312-316], but due to concerns over the stability of these compositions attention shifted towards the Ba analogues. In these materials the key concern is their stability in CO_2 containing atmospheres.

4.1 Materials for proton conducting solid oxide fuel cells (PC-SOFC)

Proton conducting ceramic fuel cells are currently considered as constituting devices with an electrolyte component from the $BaZrO_3$ and $BaCeO_3$ families that demonstrates significant proton mobility. Barium cerate has been reported as the

material with the highest proton conductivity over a wide temperature range, but has also been shown to degrade rapidly in CO_2 containing atmospheres, resulting in the formation of surface carbonate species that block the ion conduction. In order to overcome this issue the substitution of Zr for Ce was proposed[317, 318], with the $BaZrO_3$ material also showing fast proton conduction. Unfortunately the ionic transport was identified as being lower than that of the analogous cerates and a further issue discovered: dense ceramics of the zirconates were difficult to produce, requiring high temperature sintering at > 1700 ^oC. A solution to this aspect of materials development has been suggested - doping each of these compositions. Both $BaCe_{1-x}Y_xO_3$ (BCY) and $BaZr_{1-x}Y_xO_3$ (BZY) have been demonstrated as proton conducting electrolytes with later efforts directed towards solid solutions of these two materials giving electrolytes of composition Ba(Zr, Ce, Y)O_3. Several methods have been suggested to reduce the sintering temperature of these ceramics, including the use of spray pyrolysis[319] and addition of ZnO as a sintering aid[320]. The effect of the ZnO addition on the transport properties is not fully resolved.

Of course one of the advantages of the proton conductors is the relatively low temperature at which fast proton conduction is achieved, but it is also the case that many of the proton conductors have significant oxide ion conduction as well, and hence a good understanding of the temperature dependence of each of these properties is essential. Typically, the perovskites will have predominantly proton conduction until ~700 ^oC at which point oxide ion transport begins to dominate. This is of importance when considering fuel cell operation as the presence of both charge carriers can result in counter currents. A full review of the development of proton conducting ceramics for use in fuel cells is available in ref [321].

As the Ba and Sr based perovskites have some problems with processing and stability, attention has focussed on the discovery of new materials. Haugsrud et al[322-325] have suggested that the divalent substituted $LaNbO_4$ and $LaTaO_4$ series of

materials are attractive candidates. Ca-doped $LaNbO_4$ was identified as having a conductivity of 10^{-3} Scm^{-1} at 800 ^oC[323] which was the highest reported for all of the Fergusonite type lanthanides. There has also been some interest in the La_3NbO_7 material with somewhat lower conductivity (10^{-4}-10^{-3} Scm^{-1}). Each of these materials indicates that considerable scope for development PC-SOFC devices exists, and could offer a viable low temperature alternative to the IT-SOFC.

5.0 Summary

Solid oxide fuel cells consist of a complex multicomponent structure that relies heavily on inorganic materials chemistry to develop new compositions of enhanced functionality. In all aspects of both oxide ion and proton conducting based devices the structural and electrochemistry of ceramics is essential to future developments. In the preceding discussion we have highlighted a number of novel solutions for the electrolyte, anode and cathode functional components of SOFCs that overcome some of the materials limitations facing fuel cell developers. Much of this has concerned the reduction in operating temperature coupled with the durability of the materials in a wide range of operating conditions, including anode resistance to sulphur and coking. Enhanced properties may be achieved through the use of thin films of functional components, such as with yttria stabilised zirconia on $SrTiO_3$, but many questions as to the nature and origin of these enhancements remain. It is evident that there remains rich inorganic chemistry to be discovered and exploited in this vital technology area.

Tables to be included

Table 1(a) – Conductivity of typical zirconia-based fluorite electrolytes (after Singhal and Kendal, High Temperature Solid Oxide Fuel Cells, 2003, Wiley, London)

Electrolyte	Conductivity at 1000 ^{o}C (S cm^{-1})	
	As-sintered	After annealing
ZrO_2-3mol% Y_2O_3	0.059	0.05
ZrO_2-3mol% Yb_2O_3	0.063	0.09
ZrO_2-2.9mol% Sc_2O_3	0.090	0.063
ZrO_2-8mol% Y_2O_3	0.130	0.09
ZrO_2-9mol% Y_2O_3	0.130	0.12
ZrO_2-8mol% Yb_2O_3	0.200	0.15
ZrO_2-10mol% Yb_2O_3	0.150	0.15
ZrO_2-8mol% Sc_2O_3	0.300	0.12
ZrO_2-11mol% Sc_2O_3	0.300	0.30
ZrO_2-11mol% Sc_2O_3-1wt% Al_2O_3	0.260	0.26

Table 1 (b) – Conductivity of typical ceria-based fluorite electrolytes (CeO_2-Ln_2O_3)

Ln_2O_3	Mol %	Conductivity (S cm^{-1})	
		700 ^{o}C	500 ^{o}C
Sm_2O_3	10	3.5 x 10^{-2}	2.9 x 10^{-3}
Sm_2O_3	10	4.0 x 10^{-2}	5.0 x 10^{-3}
Gd_2O_3	10	3.6 x 10^{-2}	3.8 x 10^{-3}
Y_2O_3	10	1.0 x 10^{-2}	0.21 x 10^{-3}
CaO	5	2.0 x 10^{-2}	1.5 x 10^{-3}

Table 2 – Conductivity data reported for some novel perovskite oxides as potential fuel cell electrolytes.

Composition	Temperature (°C)	Conductivity (S cm^{-1})
$Nd_{0.9}Ca_{0.1}Al_{0.5}Ga_{0.5}O_{3-\delta}$	700	~10^{-2} (ref. 326)
$KNb_{0.5}Al_{0.5}O_{2.5}$	700	5.1 x 10^{-3} (ref. 327)
$KTa_{0.5}Al_{0.5}O_{2.5}$	700	2.0 x 10^{-3} (ref. 327)
$NaNb_{0.5}Al_{0.5}O_{2.5}$	700	1.5 x 10^{-3} (ref. 327)
$NaTa_{0.5}Al_{0.5}O_{2.5}$	700	1.3 x 10^{-3} (ref. 327)
$La_{0.8}Sr_{0.2}Ga_{0.9}Mg_{0.1}O_{3-\delta}$	700	7.14 x 10^{-2} (ref. 328)
$La_{0.8}Sr_{0.2}Ga_{0.85}Mg_{0.15}O_{3-\delta}$	800	0.14 (ref. 328)
$La_{0.8}Sr_{0.2}Ga_{0.83}Mg_{0.17}O_{2.815}$	700	0.079 (ref. 22)
$La_{0.8}Sr_{0.2}Ga_{0.83}Mg_{0.17}O_{2.815}$	800	0.166 (ref. 22)
$La_{0.8}Sr_{0.2}Ga_{0.85}Mg_{0.15}O_{3-\delta}$	700	0.066 (ref. 329)
$La_{0.8}Sr_{0.2}Ga_{0.85}Mg_{0.15}O_{3-\delta}$	800	0.146 (ref. 329)

Table 3 – Total conductivity and thermal expansion coefficients for $La_{1-x}Sr_xFe_{1-y}Co_yO_{3-\delta}$ ceramics in air (data from ref. 1)

x	*y*	**Total conductivity (S cm^{-1}) 873 K**	**Total conductivity (S cm^{-1}) 1073 K**	**Average TEC T (K)**	**Average TEC α x10^{-6} (K^{-1})**	**Ref.**
0	0.2	0.8	4.5	573-1173	17.5	189
0.2	0	93	1.09 x 10^2	573-1173	12.6	189
0.2	0.2	1.75 x 10^2	1.91 x 10^2	373-1173	15.4	189
0.2	0.2	1.27 x 10^2	1.49 x 10^2	373-1173	15.4	189
0.2	0.4	3.39 x 10^2	2.87 x 10^2	373-1173	17.6	189
0.2	0.6	4.14 x 10^2	4.55 x 10^2	373-1173	20	189
0.2	0.8	1.05 x 10^3	9.95 x 10^2	373-1173	20.7	189
0.2	1.0	1.69 x 10^3	1.52 x 10^3	303-1273	18.5	330
0.4	0.2	3.35 x 10^2	2.79 x 10^2	373-873	15.3	189
0.4	0.2	2.75 x 10^2	3.33 x 10^2	303-1273	17.5	330
0.4	0.2	4.60 x 10^2	3.30 x 10^2	973	15.3	190
0.6	1.0	1.81 x 10^3	1.16 x 10^3	303-1273	25.1	330
0.7	0.6	1.73 x 10^2	1.29 x 10^2	303-1273	24.1	330
0.7	0.8	4.80 x 10^2	3.88 x 10^2	303-1273	21.0	330
0.8	1.0	8.10x 10^2	5.78 x 10^2	303-1273	25.6	330

Table 4 – Electrochemical performance of metal-YSZ cermets produced by co-precipitation, after Grgicak et al.[286] Samples prepared at different pH values.

Sample	R1 / ohm cm^{-2}	R2 / ohm cm^{-2}	R3 / ohm cm^{-2}
Ni-YSZ-2	9	11	36
Ni-YSZ-3	14	46	21
Cu-YSZ-3	31	55	95
Cu-YSZ-5	10	28	38
Co-YSZ-2	7	15	20
Co-YSZ-3	4	1	15

Figures to be included.

Figure 1 – Schematic representation of two solid oxide fuel cell designs (a) Planar and (b) integrated planar.

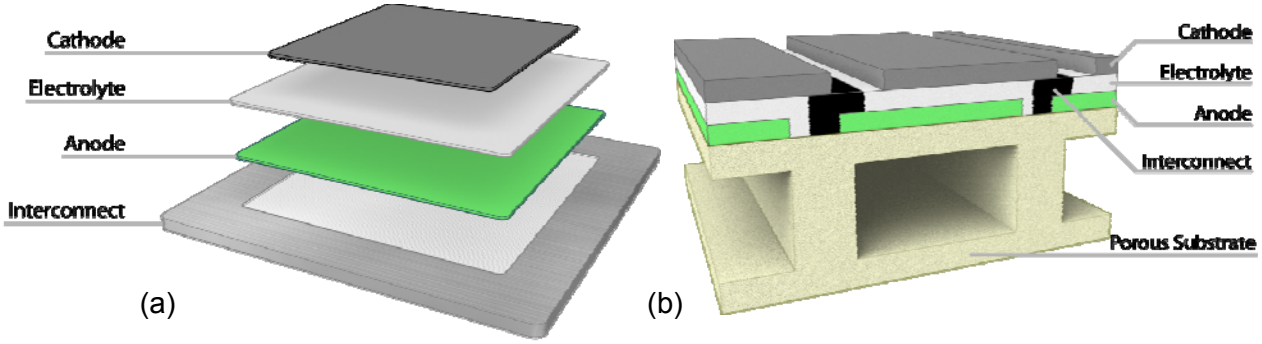

Figure 2 – Schematic representation of the (a) cubic and (b) tetragonal polymorphs of the fluorite structured yttria stabilised zirconia. Metal ions in grey, oxygen in red.

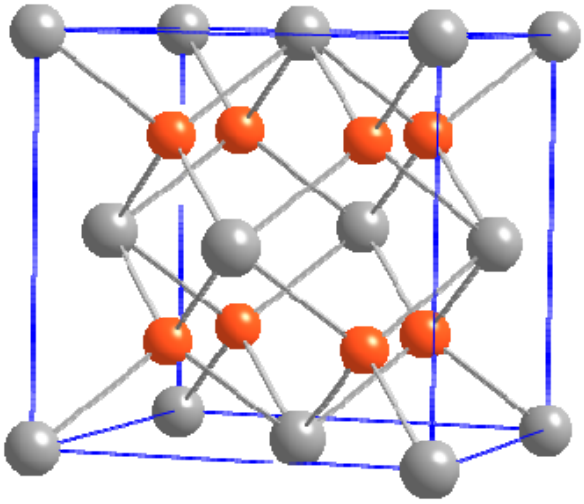

(a)

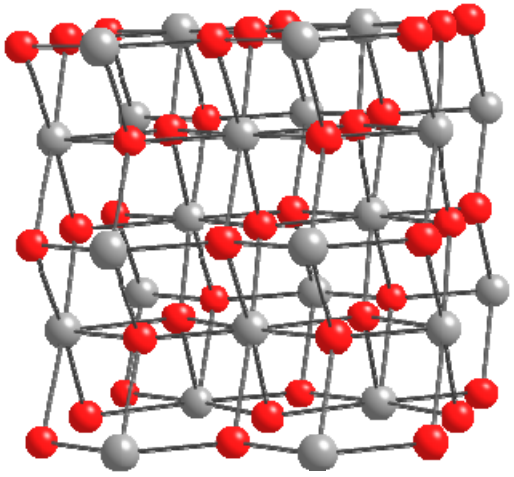

(b)

Figure 3 – Representation of the perovskite structure adopted by $LaGaO_3$-based electrolytes. Ga ions are located at the centre of the shaded octahedra.

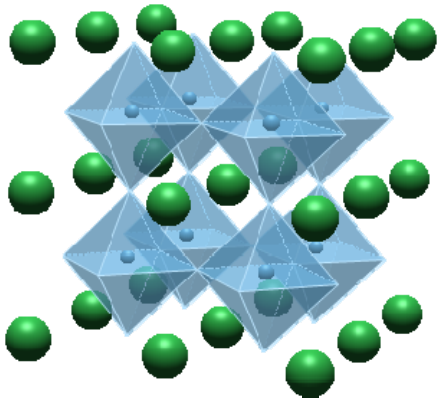

Figure 4 – Conductivity of conventional oxide ion conducting electrolytes. Data obtained from ref [2]

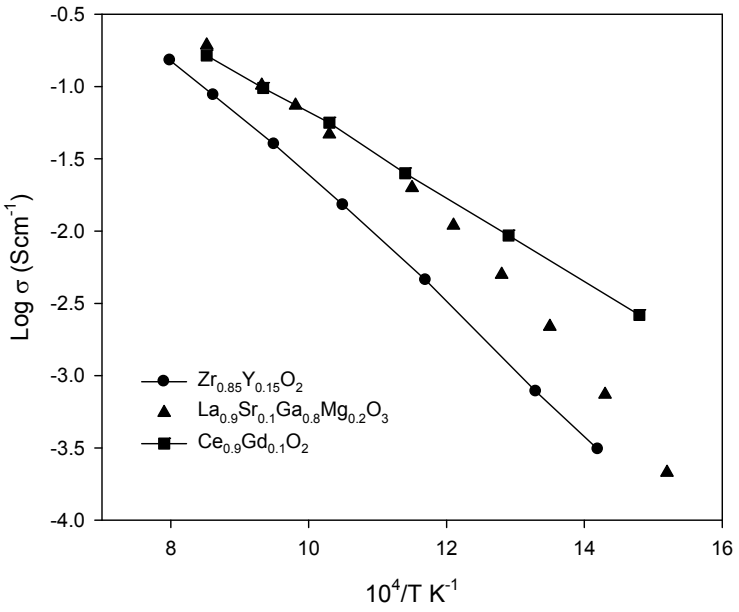

Figure 5 – Schematic illustration of electrolyte-cathode three phase boundary, typical of high temperature YSZ based SOFCs.

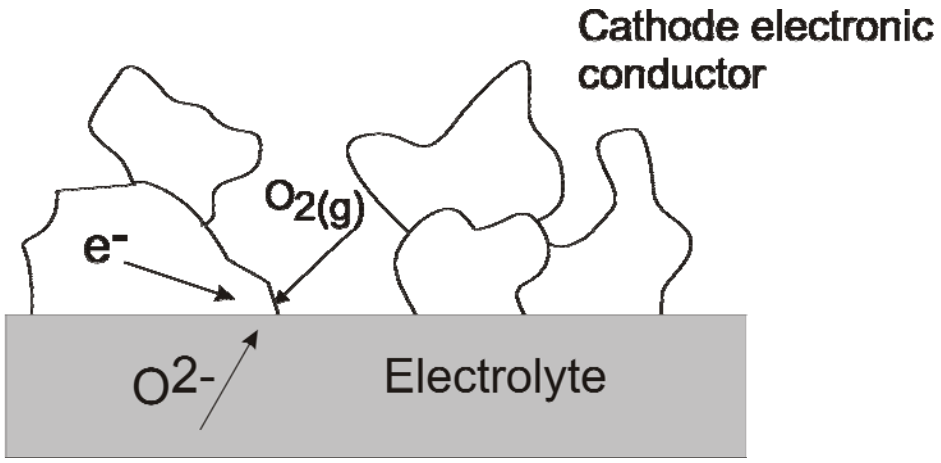

Figure 6 – Illustration of the conductivity of LSGM type electrolytes as a function of composition (data from ref. 7)

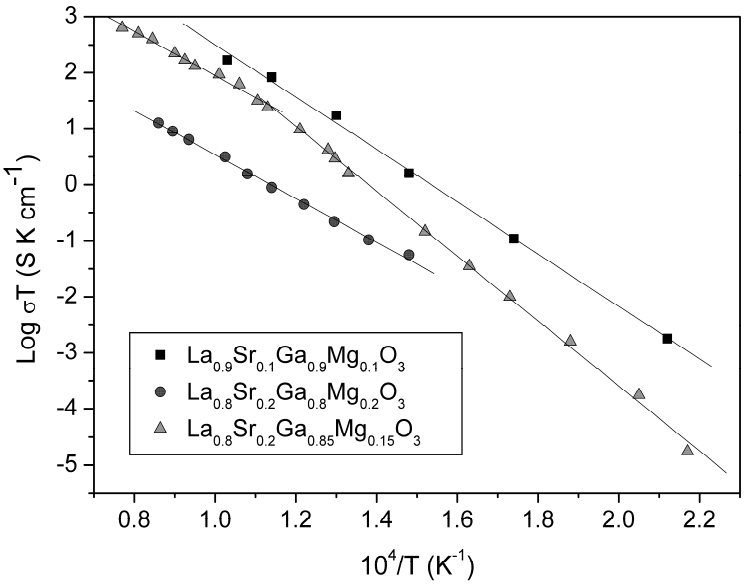

Figure 7 – Illustration of the ionic conductivity data for different compositions of cobalt- (left) and iron- (right) doped LSGM electrolytes. (published with permission from J. Electrochem. Soc.)[25]

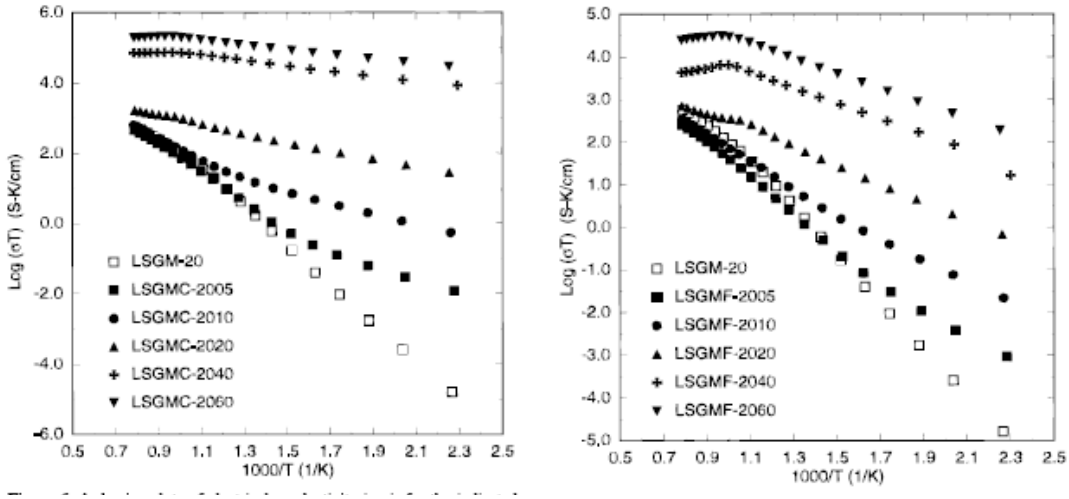

Figure 8 – Total conductivity of the ionic conductor $La_2Mo_2O_9$ highlighting the drop in conductivity associated with an α-β phase change. For comparison, A and B represent the conductivity of the stabilized zirconias $(ZrO_2)_{0.87}(CaO)_{0.13}$ and $(ZrO_2)_{0.9}(Y_2O_3)_{0.13}$ respectively (published with permission from Nature)[72]

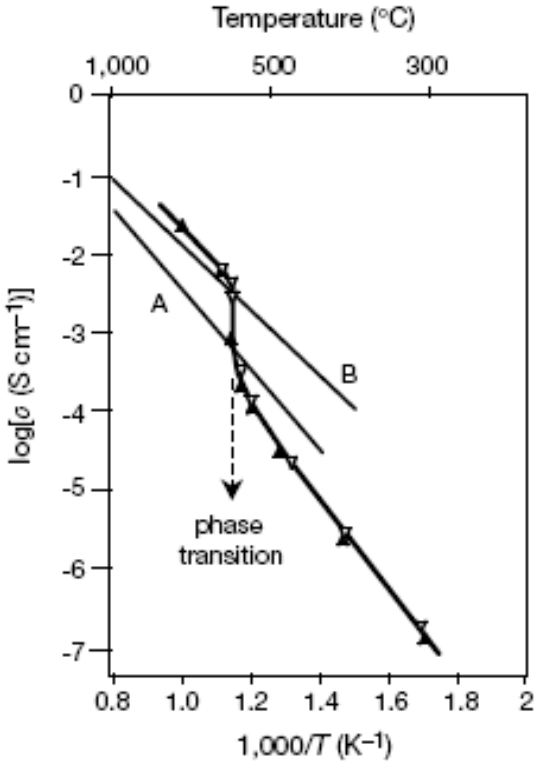

Figure 9 – Representation of the structure of (a) β–$SnWO_4$ and (b) β–$La_2Mo_2O_9$. The coordination environment of the Mo site and atomic displacement parameters of oxygens in (b) are highlighted (published with permission from Chem. Mater.)[74]

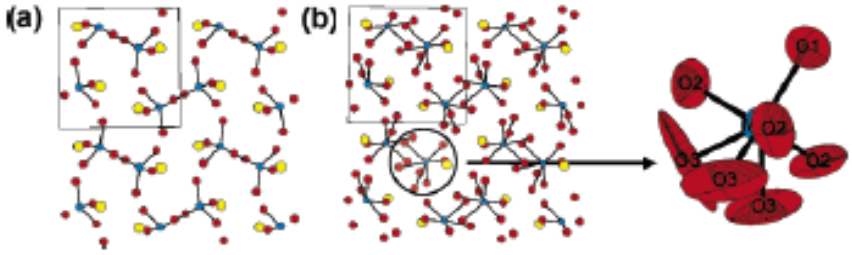

Figure 10 – Representation of the Brownmillerite structure adopted by the $Ba_2In_2O_5$. Ba atoms are represented in yellow and In atoms are located at the centre of both tetrahedra and octahedra.

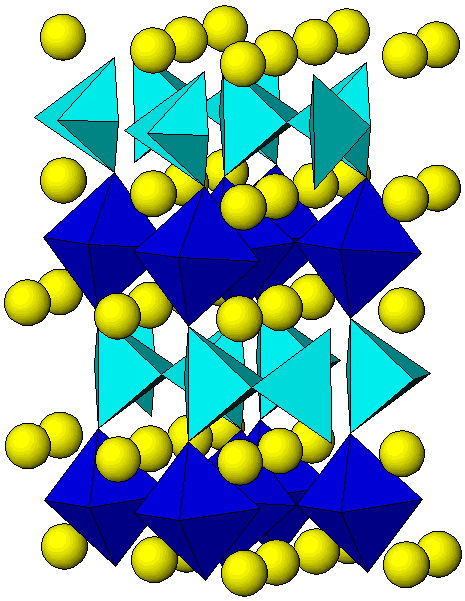

Figure 11– Total conductivity of $Ba_2In_2O_5$ and other related compounds (data from ref. 91). YSZ is included as a solid line for comparison.

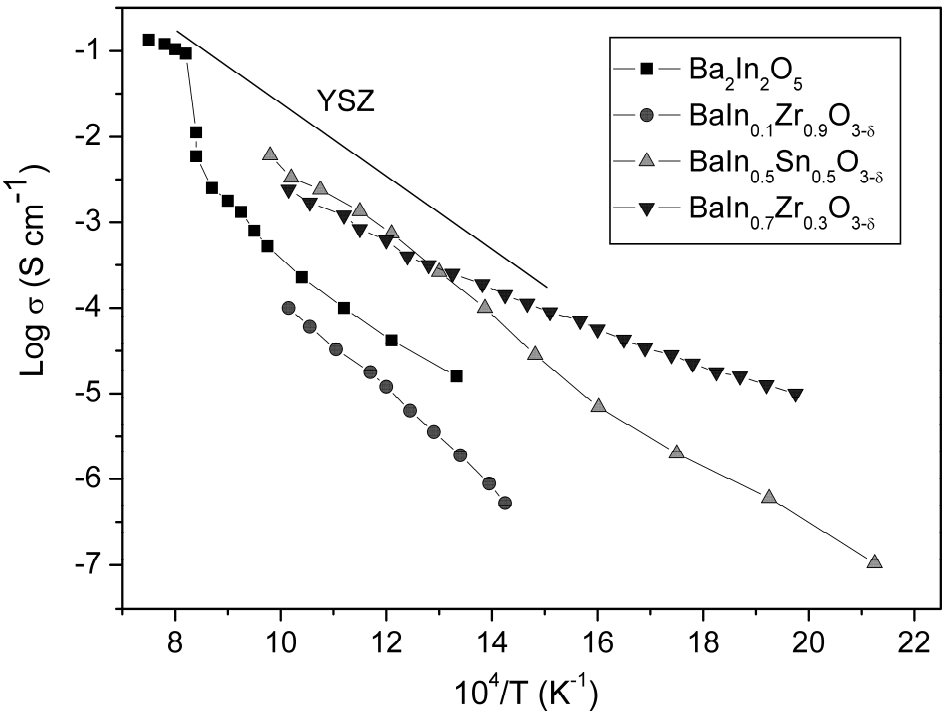

Figure 12 – Illustration showing the formation range of the cubic and rhombohedral phases as a function of the ionic radius in the Bi_2O_3-M_2O_3 system (published with permission from J. Solid State Chem)[114]

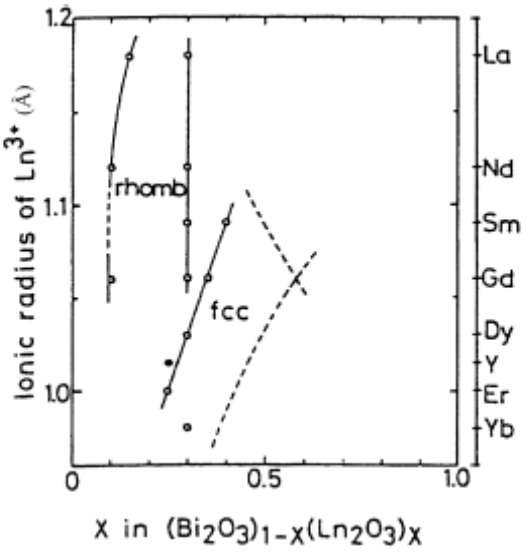

Figure 13 – Conductivity data of some typical $Bi_{1-x}Ln_xO_{1.5}$ compounds compared with YSZ and BiMeVOX families (published with permission from Chem. Rev.)[117]

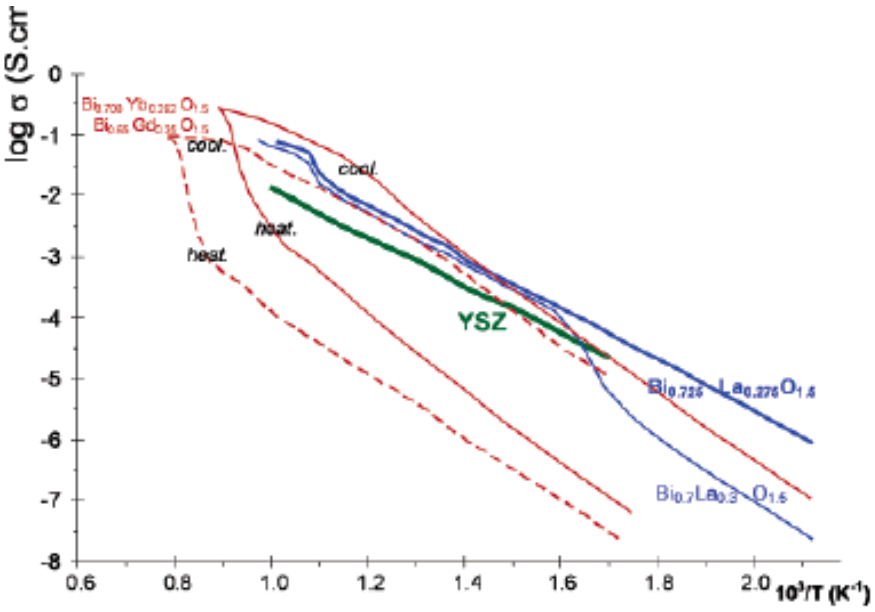

Figure 14 – Conductivity data of the $Bi_{12.5}La_{1.5}ReO_{24.5}$ and other related compounds (data from ref. 127)

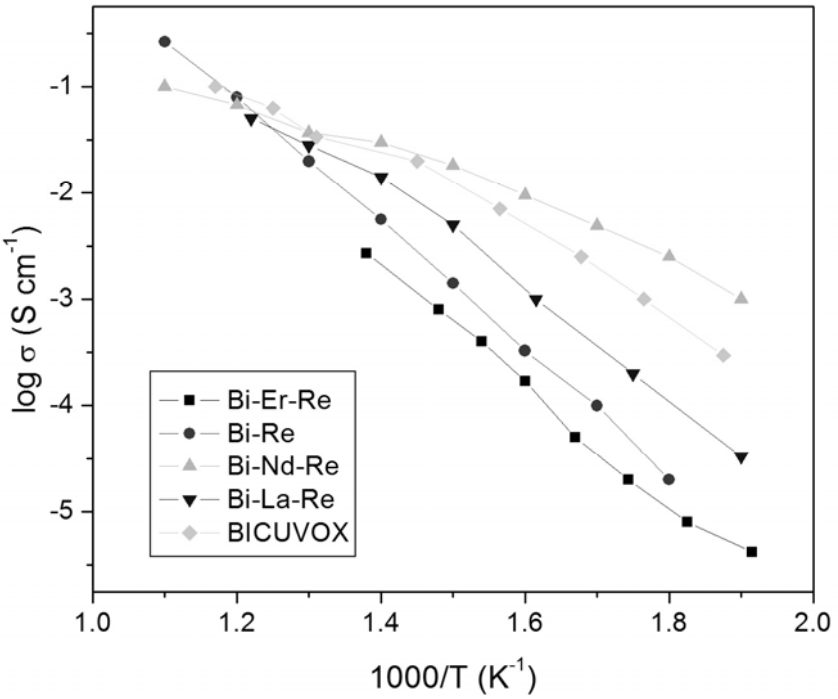

Figure 15 – Representation of the Apatite structure adopted by the $A_{10}(MO_4)_6O_{2\pm\delta}$. A atoms are represented in blue, oxygen atoms are represented in red and M atoms are located at the centre of the tetrahedra.

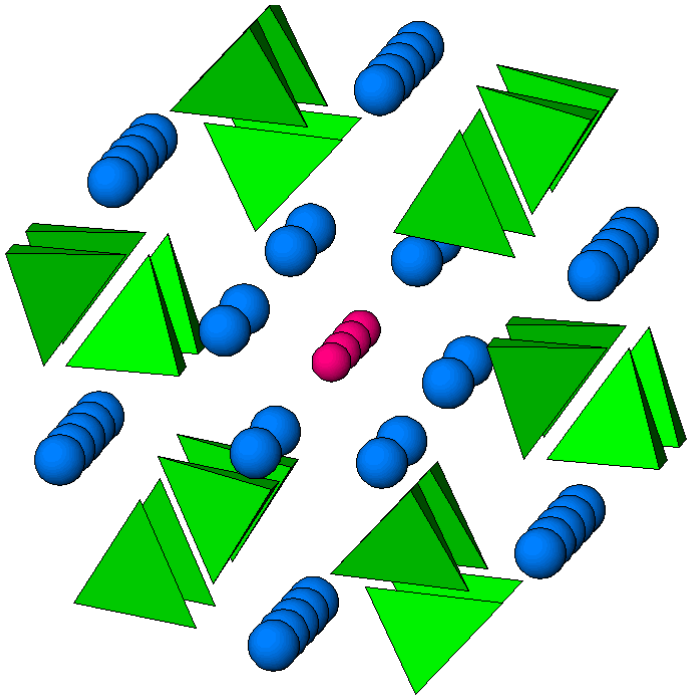

Figure 16 – Representation of the structure adopted by the $LaBaGaO_4$. La atoms are represented in blue, Ba atoms are represented in green and Ga atoms are located at the centre of the tetrahedra.

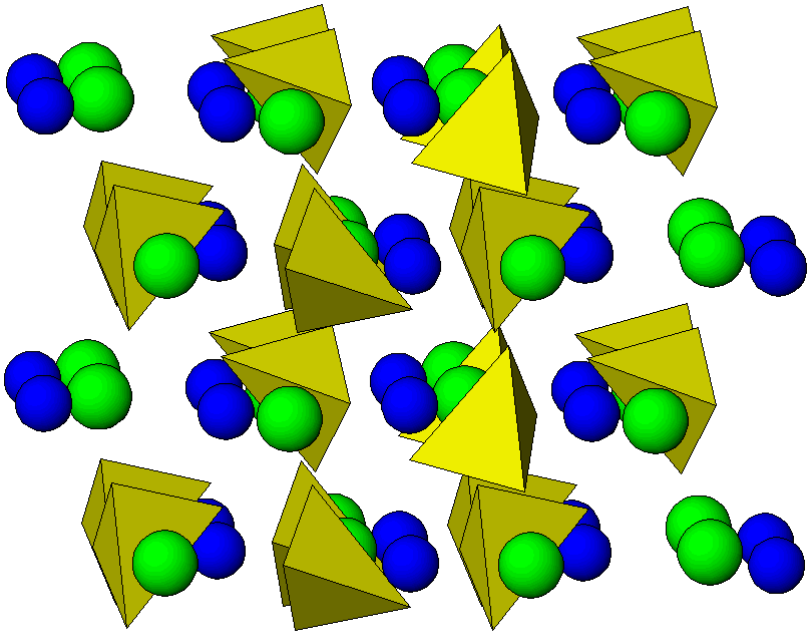

Figure 17 – Illustration of the cathodic overpotentials of porous $Ln_{0.6}Sr_{0.4}O_3$/YSZ electrodes as a function of the Ln^{3+} cationic radius (published with permission from J. Solid State Electrochem.)[1]

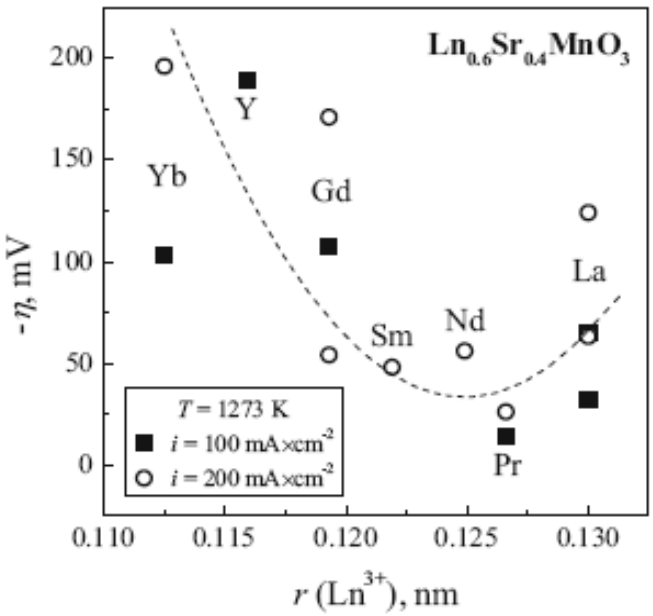

Figure 18 – Representation of the K_2NiF_4-type (A_2MO_4) structure. A atoms are represented in blue, oxygen atoms are represented in red and M atoms are located at the centre of the octahedra.

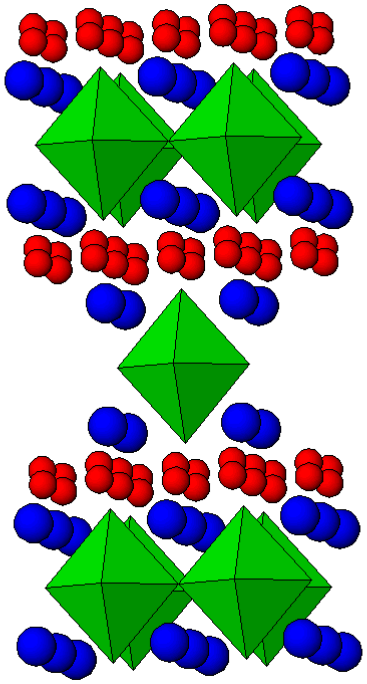

Figure 19 – Representation of the (a) crystal structure and (b) isosurface of nuclear density at 0.05 fm Á$^{-3}$ for the $(Pr_{0.9}La_{0.1})_2(Ni_{0.74}Cu_{0.21}Ga_{0.05})O_{4+\delta}$ compound determined in situ at 1015.6 ºC (published with permission from J. Am. Chem. Soc.)[201]

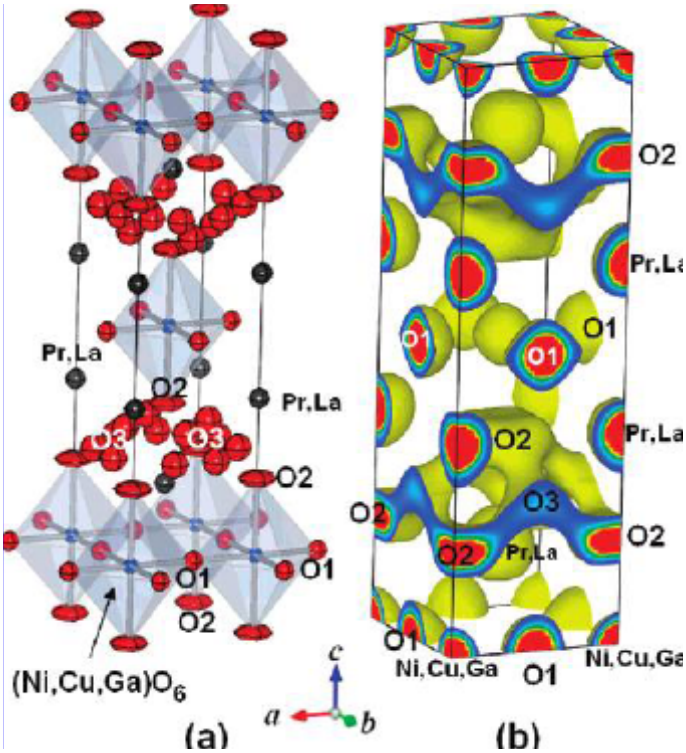

Figure 20 – Illustration of the area-specific polarization resistance as a function of the temperature for different porous oxide cathodes in air. All data correspond to electrochemical cells with YSZ electrolytes, except for $La_2Ni_{0.9}Co_{0.1}O_{4+\delta}$ and $La_2Ni_{0.8}Cu_{0.2}O_{4+\delta}$, where LSGM electrolytes were used (published with permission from J. Solid State Electrochem.)[1]

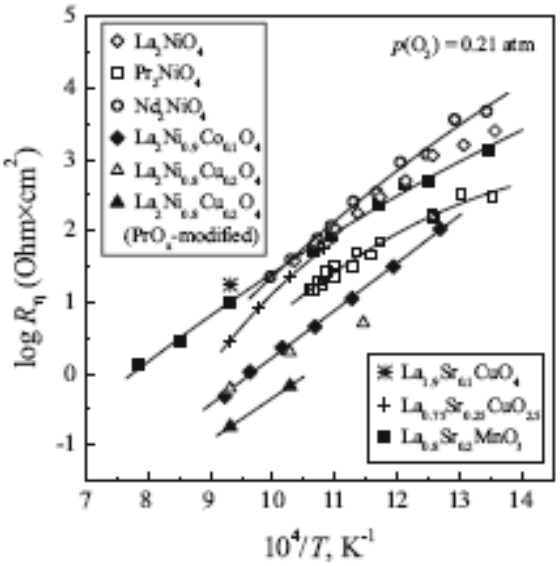

Figure 21. – Illustration of the decomposition temperature of $CeNbO_{4+\delta}$ as a function of the partial pressure of oxygen (data taken from ref. 224)

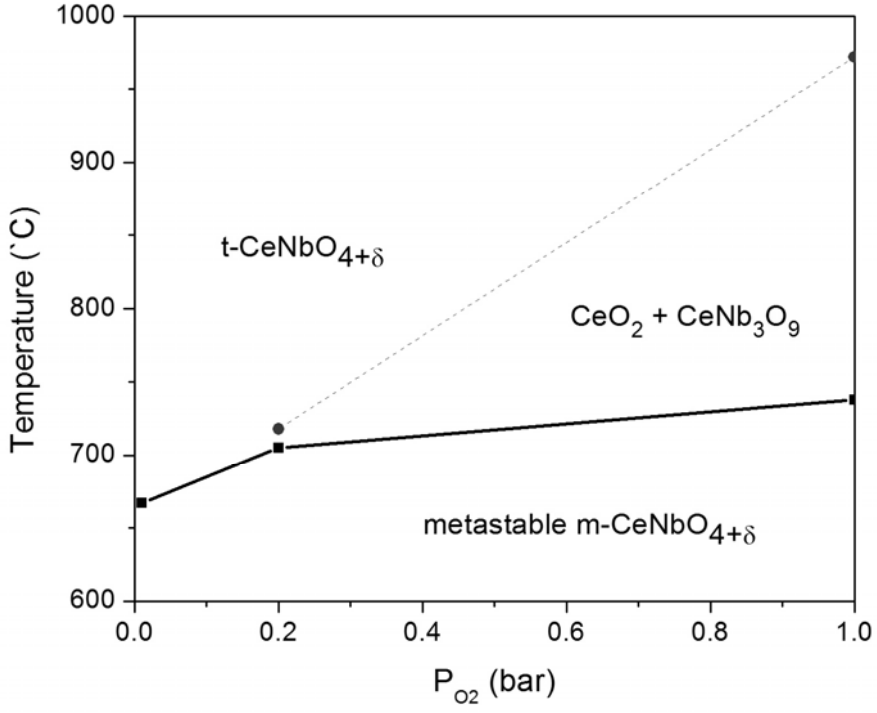

Figure 22 – Representation of the double perovskite structure adopted by the $GdBaCo_2O_5$. Gd atoms are represented in yellow, Ba atoms are represented in green and Co atoms are located at the centre of the tetrahedra.

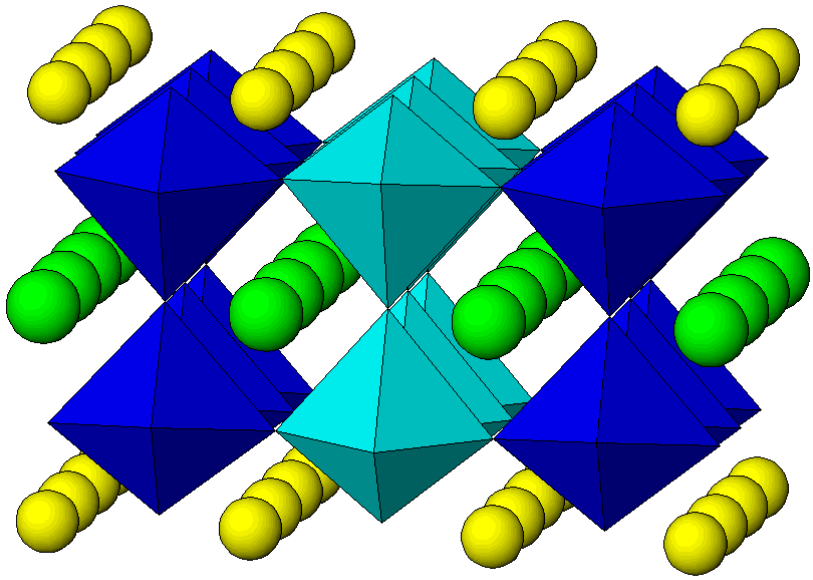

Figure 23 – SEM Image showing the incorporation of Cu by infiltration into a novel anode. (with permission from ref [270])

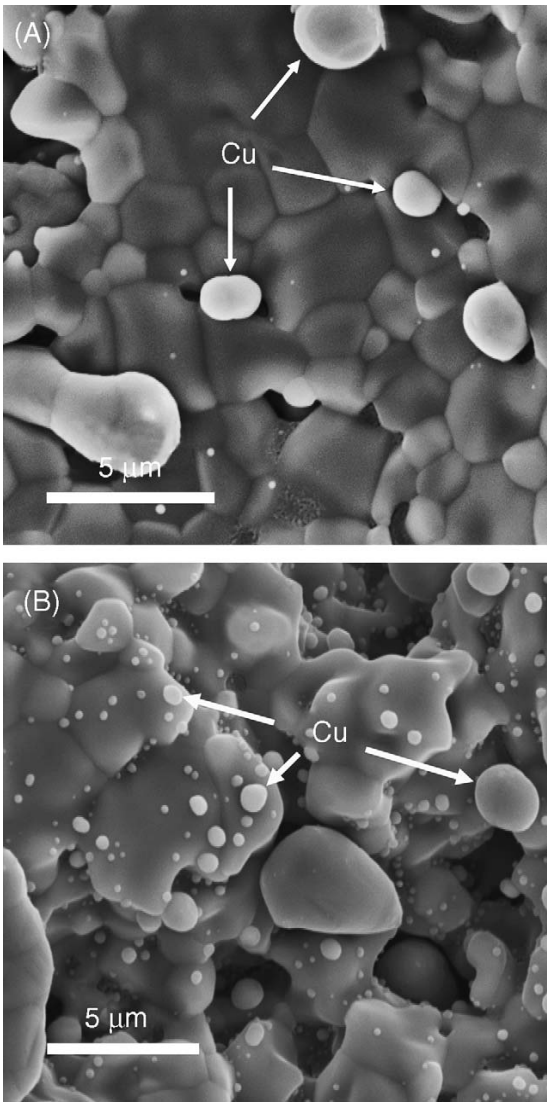

Figure 24 – Fuel cell performance curves for a YSZ based SOFC with a Cu impregnated anode. Open squares are data with a ceria layer, open circles are data obtained from a cell without the ceria layer. With permission from The Electrochemical Society in ref [271]

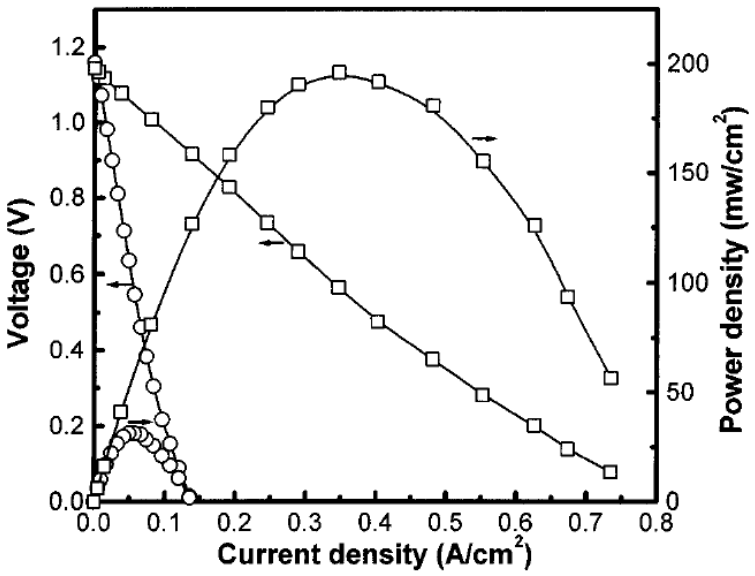

Figure 25 – X-ray absorption spectra (XAS) highlighting the redox behaviour of LSCM compositions identifying the Mn site as most active. (with permission from ref 301)

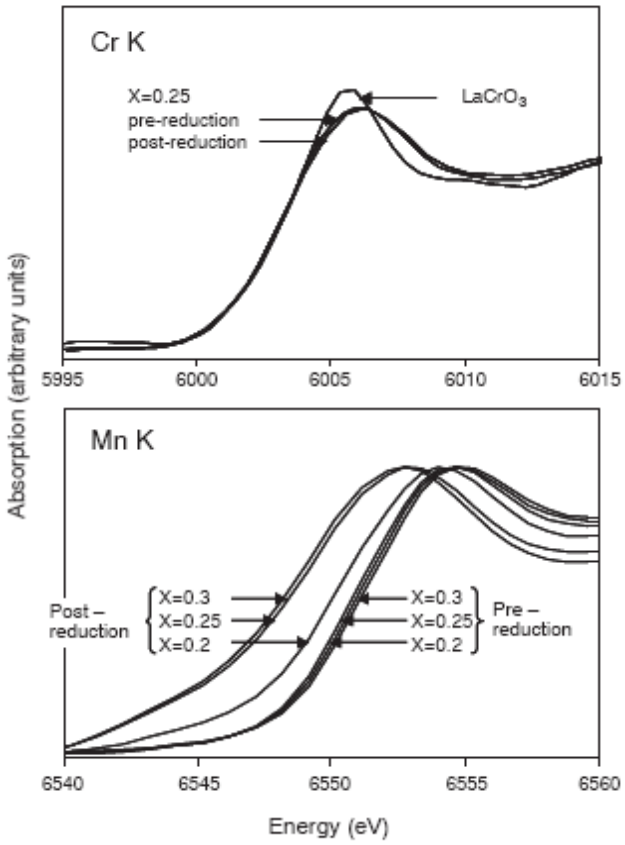

References

1. E. V. Tsipis and V. V. Kharton, *Journal of Solid State Electrochemistry*, 2008, **12**, 1367-1391.

2. E. V. Tsipis and V. V. Kharton, *J. Solid State Electrochem.*, 2008, **12**, 1039-1060.

3. J. Fleig, *Annual Review of Materials Research*, 2003, **33**, 361-382.

4. S. B. Adler, *Chemical Reviews*, 2004, **104**, 4791-4843.

5. N. P. Brandon, S. Skinner and B. C. H. Steele, *Annual Review of Materials Research*, 2003, **33**, 183-213.

6. J. B. Goodenough, *Annual Review of Materials Research*, 2003, **33**, 91-128.

7. J. W. Fergus, *Journal of Power Sources*, 2006, **162**, 30-40.

8. L. J. Gauckler, D. Beckel, B. E. Buergler, E. Jud, U. R. Muecke, M. Prestat, J. L. M. Rupp and J. Richter, *Chimia*, 2004, **58**, 837-850.

9. L. Gao and L. C. Guo, *Journal of Rare Earths*, 2005, **23**, 617-627.

10. P. Holtappels, U. Vogt and T. Graule, *Advanced Engineering Materials*, 2005, **7**, 292-302.

11. J. P. P. Huijsmans, *Current Opinion in Solid State & Materials Science*, 2001, **5**, 317-323.

12. E. Baur and H. Preis, *Z. Elektrochem.*, 1937, **43**, 727.

13. S. P. S. Badwal, F. T. Ciacchi and D. Milosevic, *Solid State Ionics*, 2000, **136**, 91-99.

14. T. Horita, N. Sakai, H. Yokokawa, M. Dokiya, T. Kawada, J. Van Herle and K. Sasaki, *Journal of Electroceramics*, 1997, **1**, 155-164.

15. S. Q. Hui, J. Roller, S. Yick, X. Zhang, C. Deces-Petit, Y. S. Xie, R. Maric and D. Ghosh, *Journal of Power Sources*, 2007, **172**, 493-502.

16. T. Ishihara, H. Matsuda and Y. Takita, *Journal of the American Chemical Society*, 1994, **116**, 3801-3803.

17. T. Ishihara, H. Matsuda and Y. Takita, *Solid State Ionics*, 1995, **79**, 147-151.

18. T. Ishihara, H. Minami, H. Matsuda, H. Nishiguchi and Y. Takita, *Chemical Communications*, 1996, 929-930.

19. T. Ishihara, H. Matsuda, M. A. binBustam and Y. Takita, *Solid State Ionics*, 1996, **86-8**, 197-201.

20. T. Ishihara, J. A. Kilner, M. Honda and Y. Takita, *Journal of the American Chemical Society*, 1997, **119**, 2747-2748.

21. K. Q. Huang, M. Feng and J. B. Goodenough, *Journal of the American Ceramic Society*, 1996, **79**, 1100-1104.

22. K. Q. Huang, R. S. Tichy and J. B. Goodenough, *Journal of the American Ceramic Society*, 1998, **81**, 2565-2575.

23. K. Q. Huang, R. S. Tichy and J. B. Goodenough, *Journal of the American Ceramic Society*, 1998, **81**, 2576-2580.

24. K. Q. Huang, R. Tichy and J. B. Goodenough, *Journal of the American Ceramic Society*, 1998, **81**, 2581-2585.

25. J. W. Stevenson, K. Hasinska, N. L. Canfield and T. R. Armstrong, *Journal of the Electrochemical Society*, 2000, **147**, 3213-3218.

26. T. Ishihara, S. Ishikawa, C. Y. Yu, T. Akbay, K. Hosoi, H. Nishiguchi and Y. Takita, *Physical Chemistry Chemical Physics*, 2003, **5**, 2257-2263.

27. A. Atkinson, S. Barnett, R. J. Gorte, J. T. S. Irvine, A. J. McEvoy, M. Mogensen, S. C. Singhal and J. Vohs, *Nature Materials*, 2004, **3**, 17-27.

28. S. P. Jiang and S. H. Chan, *Journal of Materials Science*, 2004, **39**, 4405-4439.

29. S. Primdahl and M. Mogensen, *Journal of Applied Electrochemistry*, 2000, **30**, 247-257.

30. D. Sarantaridis and A. Atkinson, *Fuel Cells*, 2007, **7**, 246-258.

31. V. Alzate-Restrepo and J. M. Hill, *Applied Catalysis a-General*, 2008, **342**, 49-55.

32. D. J. L. Brett, A. Atkinson, N. P. Brandon and S. J. Skinner, *Chemical Society Reviews*, 2008, **37**, 1568-1578.

33. A. Lashtabeg and S. J. Skinner, *Journal of Materials Chemistry*, 2006, **16**, 3161-3170.

34. S. J. Skinner, *International Journal of Inorganic Materials*, 2001, **3**, 113-121.

35. B. C. H. Steele, *Solid State Ionics*, 2000, **134**, 3-20.

36. S. P. Jiang, *Journal of Materials Science*, 2008, **43**, 6799-6833.

37. A. Chen, G. Bourne, K. Siebein, R. DeHoff, E. Wachsman and K. Jones, *Journal of the American Ceramic Society*, 2008, **91**, 2670-2675.

38. A. Grosjean, O. Sanseau, V. Radmilovic and A. Thorel, 15th International Conference on Solid State Ionics, Baden Baden, GERMANY, 2006.

39. P. Ried, P. Holtappels, A. Wichser, A. Ulrich and T. Graule, *Journal of the Electrochemical Society*, 2008, **155**, B1029-B1035.

40. X. Y. Chen, J. S. Yu and S. B. Adler, *Chemistry of Materials*, 2005, **17**, 4537-4546.

41. V. Dusastre and J. A. Kilner, *Solid State Ionics*, 1999, **126**, 163-174.

42. Z. P. Shao and S. M. Haile, *Nature*, 2004, **431**, 170-173.

43. W. Zhou, R. Ran, Z. P. Shao, W. Zhuang, J. Jia, H. X. Gu, W. Q. Jin and N. P. Xu, *Acta Materialia*, 2008, **56**, 2687-2698.

44. H. L. Zhao, W. Shen, Z. M. Zhu, X. Li and Z. F. Wang, *Journal of Power Sources*, 2008, **182**, 503-509.

45. Y. Zhang, J. Liu, X. Huang, Z. Lu and W. Su, *Solid State Ionics*, 2008, **179**, 250-255.

46. A. Y. Yan, M. Yang, Z. F. Hou, Y. L. Dong and M. J. Cheng, *Journal of Power Sources*, 2008, **185**, 76-84.

47. J. Pena-Martinez, D. Marrero-Lopez, J. C. Ruiz-Morales, B. E. Buergler, P. Nunez and L. J. Gauckler, *Solid State Ionics*, 2006, **177**, 2143-2147.

48. Y. Lin, R. Ran, Y. Zheng, Z. P. Shao, W. Q. Jin, N. P. Xu and J. M. Ahn, *Journal of Power Sources*, 2008, **180**, 15-22.

49. Z. S. Duan, M. Yang, A. Yan, Z. F. Hou, Y. L. Dong, Y. Chong, M. J. Cheng and W. S. Yang, *Journal of Power Sources*, 2006, **160**, 57-64.

50. M. Arnold, T. M. Gesing, J. Martynczuk and A. Feldhoff, *Chemistry of Materials*, 2008, **20**, 5851-5858.

51. C. R. Xia, W. Rauch, F. L. Chen and M. L. Liu, *Solid State Ionics*, 2002, **149**, 11-19.

52. Z. L. Tang, Y. S. Xie, H. Hawthorne and D. Ghosh, *Journal of Power Sources*, 2006, **157**, 385-388.

53. H. Lv, Y. J. Wu, B. Huang, B. Y. Zhao and K. A. Hu, *Solid State Ionics*, 2006, **177**, 901-906.

54. M. Koyama, C. J. Wen, T. Masuyama, J. Otomo, H. Fukunaga, K. Yamada, K. Eguchi and H. Takahashi, *Journal of the Electrochemical Society*, 2001, **148**, A795-A801.

55. H. Fukunaga, M. Koyama, N. Takahashi, C. Wen and K. Yamada, *Solid State Ionics*, 2000, **132**, 279-285.

56. T. Takahashi and H. Iwahara, *Energy Convers.*, 1971, **11**, 105-111.

57. M. Kajitani, M. Matsuda and M. Miyake, *Solid State Ionics*, 2006, **177**, 1721-1724.

58. J. W. Stevenson, T. R. Armstrong, D. E. McCready, I. R. Pederson and W. J. Weber, *Journal of the Electrochemical Society*, 1997, **144**, 3613-3620.

59. J. Bradley, P. R. Slater, T. Ishihara and J. T. S. Irvine, *Solid Oxide Fuel Cells Viii (Sofc Viii)*, 2003, **2003**, 315-323.

60. V. Thangadurai and W. Weppner, *Journal of the Electrochemical Society*, 2001, **148**, A1294-A1301.

61. D. Lybye, F. W. Poulsen and M. Mogensen, *Solid State Ionics*, 2000, **128**, 91-103.

62. T. Ishihara, H. Furutani, M. Honda, T. Yamada, T. Shibayama, T. Akbay, N. Sakai, H. Yokokawa and Y. Takita, *Chemistry of Materials*, 1999, **11**, 2081-2088.

63. B. A. Khorkounov, H. Nafe and F. Aldinger, *Journal of Solid State Electrochemistry*, 2006, **10**, 479-487.

64. T. Ishihara, J. Tabuchi, S. Ishikawa, J. Yan, M. Enoki and H. Matsumoto, *Solid State Ionics*, 2006, **177**, 1949-1953.

65. M. Enoki, J. W. Yan, H. Matsumoto and T. Ishihara, *Solid State Ionics*, 2006, **177**, 2053-2057.

66. A. A. Yaremchenko, V. V. Kharton, E. N. Naumovich, D. I. Shestakov, V. F. Chukharev, A. V. Kovalevsky, A. L. Shaula, M. V. Patrakeev, J. R. Frade and F. M. B. Marques, *Solid State Ionics*, 2006, **177**, 549-558.

67. N. S. Chae, K. S. Park, Y. S. Yoon, I. S. Yoo, J. S. Kim and H. H. Yoon, *Colloids and Surfaces a-Physicochemical and Engineering Aspects*, 2008, **313**, 154-157.

68. R. Polini, A. Falsetti, E. Traversa, O. Schaf and P. Knauth, *Journal of the European Ceramic Society*, 2007, **27**, 4291-4296.

69. B. W. Liu and Y. Zhang, *Journal of Alloys and Compounds*, 2008, **458**, 383-389.

70. V. Thangadurai, P. S. Beurmann and W. Weppner, *Materials Science and Engineering B-Solid State Materials for Advanced Technology*, 2003, **100**, 18-22.

71. S. Hashimoto, H. Kishimoto and H. Iwahara, *Solid State Ionics*, 2001, **139**, 179-187.

72. P. Lacorre, F. Goutenoire, O. Bohnke, R. Retoux and Y. Laligant, *Nature*, 2000, **404**, 856-858.

73. L. Malavasi, H. Kim, S. J. L. Billinge, T. Proffen, C. Tealdi and G. Flor, *Journal of the American Chemical Society*, 2007, **129**, 6903-6907.

74. I. R. Evans, J. A. K. Howard and J. S. O. Evans, *Chemistry of Materials*, 2005, **17**, 4074-4077.

75. F. Goutenoire, O. Isnard, R. Retoux and P. Lacorre, *Chemistry of Materials*, 2000, **12**, 2575-2580.

76. P. Lacorre, *Solid State Sciences*, 2000, **2**, 755-758.

77. S. Georges, F. Goutenoire, O. Bohnke, M. C. Steil, S. J. Skinner, H. D. Wiemhofer and P. Lacorre, *Journal of New Materials for Electrochemical Systems*, 2004, **7**, 51-57.

78. J. A. Collado, M. A. G. Aranda, A. Cabeza, P. Olivera-Pastor and S. Bruque, *Journal of Solid State Chemistry*, 2002, **167**, 80-85.

79. Z. S. Khadasheva, N. U. Venskovskii, M. G. Safronenko, A. V. Mosunov, E. D. Politova and S. Y. Stefanovich, *Inorganic Materials*, 2002, **38**, 1168-1171.

80. S. Basu, P. S. Devi and H. S. Maiti, *Journal of the Electrochemical Society*, 2005, **152**, A2143-A2147.

81. S. Georges, F. Goutenoire, F. Altorfer, D. Sheptyakov, F. Fauth, E. Suard and P. Lacorre, *Solid State Ionics*, 2003, **161**, 231-241.

82. S. Basu, P. S. Devi and H. S. Maiti, *Applied Physics Letters*, 2004, **85**, 3486-3488.

83. D. Marrero-Lopez, D. Perez-Coll, J. C. Ruiz-Morales, J. Canales-Vazquez, M. C. Martin-Sedeno and P. Nunez, *Electrochimica Acta*, 2007, **52**, 5219-5231.

84. S. Georges, S. J. Skinner, P. Lacorre and M. C. Steil, *Dalton Transactions*, 2004, 3101-3105.

85. J. H. Yang, Z. Y. Wen, Z. H. Gu and D. S. Yan, *Journal of the European Ceramic Society*, 2005, **25**, 3315-3321.

86. J. X. Wang, X. P. Wang, F. J. Liang, Z. J. Cheng and Q. F. Fang, *Solid State Ionics*, 2006, **177**, 1437-1442.

87. A. Subramania, T. Saradha and S. Muzhumathi, *Materials Research Bulletin*, 2008, **43**, 1153-1159.

88. J. B. Goodenough, J. E. Ruizdiaz and Y. S. Zhen, *Solid State Ionics*, 1990, **44**, 21-31.

89. A. Manthiram, J. F. Kuo and J. B. Goodenough, *Solid State Ionics*, 1993, **62**, 225-234.

90. T. Schober, *Solid State Ionics*, 1998, **109**, 1-11.

91. V. V. Kharton, F. M. B. Marques and A. Atkinson, *Solid State Ionics*, 2004, **174**, 135-149.

92. T. Kobayashi, Y. Senoo, M. Hibino and T. Yao, *Solid State Ionics*, 2006, **177**, 1743-1746.

93. A. Rolle, R. N. Vannier, N. V. Giridharan and F. Abraham, *Solid State Ionics*, 2005, **176**, 2095-2103.

94. D. H. Gregory and M. T. Weller, *Journal of Solid State Chemistry*, 1993, **107**, 134-148.

95. T. Yao, Y. Uchimoto, M. Kinuhata, T. Inagaki and H. Yoshida, *Solid State Ionics*, 2000, **132**, 189-198.

96. K. Kakinuma, H. Yamamura and T. Atake, *Journal of Thermal Analysis and Calorimetry*, 2002, **69**, 897-904.

97. V. Jayaraman, A. Magrez, M. Caldes, O. Joubert, M. Ganne, Y. Piffard and L. Brohan, *Solid State Ionics*, 2004, **170**, 17-24.

98. A. Yamaji, K. Kawakami, M. Arai and T. Adachi, *New Materials for Batteries and Fuel Cells*, 2000, **575**, 343-348.

99. K. Kakinuma, H. Yamamura, H. Haneda and T. Atake, *Solid State Ionics*, 2002, **154**, 571-576.

100. J. B. Goodenough, *Solid State Ionics*, 1997, **94**, 17-25.

101. G. GATTOW and SCHRÖDER, *ZEITSCHRIFT FÜR ANORGANISCHE UND ALLGEMEINE CHEMIE*, 1962, **318**, 176-189.

102. M. Yashima and D. Ishimura, *Chemical Physics Letters*, 2003, **378**, 395-399.

103. T. Takahashi, H. Iwahara and T. Arao, *Journal of Applied Electrochemistry*, 1975, **5**, 187-195.

104. A. Watanabe and T. Kikuchi, *Solid State Ionics*, 1986, **21**, 287-291.

105. H. Mizoguchi, K. Ueda, H. Kawazoe, H. Hosono, T. Omata and S. Fujitsu, *Journal of Materials Chemistry*, 1997, **7**, 943-946.

106. M. J. Verkerk, K. Keizer and A. J. Burggraaf, *Journal of Applied Electrochemistry*, 1980, **10**, 81-90.

107. J. R. Jurado, C. Moure, P. Duran and N. Valverde, *Solid State Ionics*, 1988, **28**, 518-523.

108. M. J. Verkerk and A. J. Burggraaf, *Journal of the Electrochemical Society*, 1981, **128**, 75-82.

109. A. Watanabe, *Solid State Ionics*, 1995, **79**, 84-88.

110. H. CAHEN, T. VAN DEN BELT, J. DE WIT and G. BROERS, *SOLID STATE IONICS*, 1980, **1**, 411-423.

111. T. Takahashi, H. Iwahara and T. Esaka, *Journal of the Electrochemical Society*, 1977, **124**, 1563-1569.

112. A. Watanabe and A. Ono, *Solid State Ionics*, 2004, **174**, 15-18.

113. N. M. Sammes, G. A. Tompsett, H. Nafe and F. Aldinger, *Journal of the European Ceramic Society*, 1999, **19**, 1801-1826.

114. H. Iwahara, T. Esaka, T. Sato and T. Takahashi, *Journal of Solid State Chemistry*, 1981, **39**, 173-180.

115. T. TAKAHASHI, H. IWAHARA and Y. NAGAI, *JOURNAL OF APPLIED ELECTROCHEMISTRY*, 1972, **2**, 97-104.

116. D. Mercurio, M. Elfarissi, J. C. Champarnaudmesjard, B. Frit, P. Conflant and G. Roult, *Journal of Solid State Chemistry*, 1989, **80**, 133-143.

117. M. Drache, P. Roussel and J. P. Wignacourt, *Chemical Reviews*, 2007, **107**, 80-96.

118. A. Watanabe, *Solid State Ionics*, 1990, **40-1**, 889-892.

119. A. Watanabe, *Solid State Ionics*, 1996, **86-8**, 1427-1430.

120. K. Z. Fung, J. Chen and A. V. Virkar, *Journal of the American Ceramic Society*, 1993, **76**, 2403-2418.

121. N. X. Jiang and E. D. Wachsman, *Journal of the American Ceramic Society*, 1999, **82**, 3057-3064.

122. A. Watanabe and M. Sekita, *Solid State Ionics*, 2005, **176**, 2429-2433.

123. F. Krok, I. Abrahams, W. Wrobel, S. C. M. Chan, A. Kozanecka, T. Ossowski and J. R. Dygas, 14th International Conference on Solid State Ionics, Monterey, CA, 2003.

124. A. A. Yaremchenko, V. V. Kharton, E. N. Naumovich, A. A. Tonoyan and V. V. Samokhval, *Journal of Solid State Electrochemistry*, 1998, **2**, 308-314.

125. K. Laurent, G. Y. Wang, S. Tusseau-Nenez and Y. Leprince-Wang, *Solid State Ionics*, 2008, **178**, 1735-1739.

126. F. Mauvy, J. C. Launay and J. Darriet, *Journal of Solid State Chemistry*, 2005, **178**, 2015-2023.

127. R. Punn, A. M. Feteira, D. C. Sinclair and C. Greaves, *Journal of the American Chemical Society*, 2006, **128**, 15386-15387.

128. N. X. Jiang, E. D. Wachsman and S. H. Jung, *Solid State Ionics*, 2002, **150**, 347-353.

129. K. Reiselhuber, G. Dorner and M. W. Breiter, *Electrochimica Acta*, 1993, **38**, 969-973.

130. X. P. Wang, G. Corbel, Q. F. Fang and P. Lacorre, *Journal of Materials Chemistry*, 2006, **16**, 1561-1566.

131. F. Abraham, M. F. Debreuillegresse, G. Mairesse and G. Nowogrocki, *Solid State Ionics*, 1988, **28**, 529-532.

132. E. Pernot, M. Anne, M. Bacmann, P. Strobel, J. Fouletier, R. N. Vannier, G. Mairesse, F. Abraham and G. Nowogrocki, 9th International Conference on Solid State Ionics, The Hague, Netherlands, 1993.

133. J. B. Goodenough, A. Manthiram, M. Paranthaman and Y. S. Zhen, Symp on Solid State Ionics at the International Conf on Advanced Materials, Strasbourg, France, 1991.

134. A. A. Yaremchenko, V. V. Kharton, E. N. Naumovich and V. V. Samokhval, *Solid State Ionics*, 1998, **111**, 227-236.

135. E. Kendrick, M. S. Islam and P. R. Slater, *Journal of Materials Chemistry*, 2007, **17**, 3104-3111.

136. T. J. White and Z. L. Dong, *Acta Crystallographica Section B-Structural Science*, 2003, **59**, 1-16.

137. S. Nakayama, H. Aono and Y. Sadaoka, *Chemistry Letters*, 1995, 431-432.

138. S. W. Tao and J. T. S. Irvine, *Materials Research Bulletin*, 2001, **36**, 1245-1258.

139. J. E. H. Sansom, J. R. Tolchard, P. R. Slater and M. S. Islam, *Solid State Ionics*, 2004, **167**, 17-22.

140. E. J. Abram, D. C. Sinclair and A. R. West, *Journal of Materials Chemistry*, 2001, **11**, 1978-1979.

141. L. Leon-Reina, M. C. Martin-Sedeno, E. R. Losilla, A. Cabeza, M. Martinez-Lara, S. Bruque, F. M. B. Marques, D. V. Sheptyakov and M. A. G. Aranda, *Chemistry of Materials*, 2003, **15**, 2099-2108.

142. J. R. Tolchard, P. R. Slater and M. S. Islam, *Advanced Functional Materials*, 2007, **17**, 2564-2571.

143. M. S. Islam, J. R. Tolchard and P. R. Slater, *Chemical Communications*, 2003, 1486-1487.

144. L. Leon-Reina, E. R. Losilla, M. Martinez-Lara, S. Bruque and M. A. G. Aranda, *Journal of Materials Chemistry*, 2004, **14**, 1142-1149.

145. J. E. H. Sansom, J. R. Tolchard, M. S. Islam, D. Apperley and P. R. Slater, *Journal of Materials Chemistry*, 2006, **16**, 1410-1413.

146. A. Orera, E. Kendrick, D. C. Apperley, V. M. Orera and P. R. Slater, *Dalton Transactions*, 2008, 5296-5301.

147. J. E. H. Sansom, D. Richings and P. R. Slater, *Solid State Ionics*, 2001, **139**, 205-210.

148. L. Leon-Reina, E. R. Losilla, M. Martinez-Lara, S. Bruque, A. Llobet, D. V. Sheptyakov and M. A. G. Aranda, *Journal of Materials Chemistry*, 2005, **15**, 2489-2498.

149. L. Leon-Reina, J. M. Porras-Vazquez, E. R. Losilla and M. A. G. Aranda, *Journal of Solid State Chemistry*, 2007, **180**, 1250-1258.

150. A. Chesnaud, C. Bogicevic, F. Karolak, C. Estournes and G. Dezanneau, *Chemical Communications*, 2007, 1550-1552.

151. H. Arikawa, H. Nishiguchi, T. Ishihara and Y. Takita, *Solid State Ionics*, 2000, **136**, 31-37.

152. E. J. Abram, C. A. Kirk, D. C. Sinclair and A. R. West, *Solid State Ionics*, 2005, **176**, 1941-1947.

153. J. R. Tolchard, J. E. H. Sansom, P. R. Slater and M. S. Islam, OSSEP Workshop on Ionic and Mixed Conductors, Aveiro, PORTUGAL, 2003.

154. E. Kendrick, M. S. Islam and P. R. Slater, *Chemical Communications*, 2008, 715-717.

155. S. S. Pramana, W. T. Klooster and T. J. White, *Acta Crystallographica Section B-Structural Science*, 2007, **63**, 597-602.

156. E. V. Tsipis, V. V. Kharton and J. R. Frade, *Electrochimica Acta*, 2007, **52**, 4428-4435.

157. E. Kendrick, J. Kendrick, K. S. Knight, M. S. Islam and P. R. Slater, *Nature Materials*, 2007, **6**, 871-875.

158. F. Schönberger, E. Kendrick, M. S. Islam and P. R. Slater, *Solid State Ionics*, 2005, **176**, 2951-2953.

159. J. M. S. Skakle and R. Herd, *Powder Diffraction*, 1999, **14**, 195-202.

160. M. Rozumek, P. Majewski, H. Schluckwerder, F. Aldinger, K. Kunstler and G. Tomandl, *Journal of the American Ceramic Society*, 2004, **87**, 1795-1798.

161. E. S. Raj, S. J. Skinner and J. A. Kilner, *Solid State Ionics*, 2005, **176**, 1097-1101.

162. X. Kuang, M. A. Green, H. Niu, P. Zajdel, C. Dickinson, J. B. Claridge, L. Jantsky and M. J. Rosseinsky, *Nature Materials*, 2008, **7**, 498-504.

163. R. A. De Souza, M. S. Islam and E. Ivers-Tiffee, *Journal of Materials Chemistry*, 1999, **9**, 1621-1627.

164. Y. Sakaki, Y. Takeda, A. Kato, N. Imanishi, O. Yamamoto, M. Hattori, M. Iio and Y. Esaki, *Solid State Ionics*, 1999, **118**, 187-194.

165. T. L. Wen, H. Tu, Z. Xu and O. Yamamoto, *Solid State Ionics*, 1999, **121**, 25-30.

166. Y. Takeda, H. Y. Tu, H. Sakaki, S. Watanabe, N. Imanishi, O. Yamamoto, M. B. Phillipps and N. M. Sammes, *Journal of the Electrochemical Society*, 1997, **144**, 2810-2816.

167. Y. Takeda, Y. Sakaki, T. Ichikawa, N. Imanishi, O. Yamamoto, M. Mori, N. Mori and T. Abe, *Solid State Ionics*, 1994, **72**, 257-264.

168. T. Ishihara, T. Kudo, H. Matsuda and Y. Takita, *Journal of the Electrochemical Society*, 1995, **142**, 1519-1524.

169. H. R. Rim, S. K. Jeung, E. Jung and J. S. Lee, *Materials Chemistry and Physics*, 1998, **52**, 54-59.

170. M. B. Phillipps, N. M. Sammes and O. Yamamoto, *Solid State Ionics*, 1999, **123**, 131-138.

171. M. A. Pena and J. L. G. Fierro, *Chemical Reviews*, 2001, **101**, 1981-2017.

172. I. P. Marozau, V. V. Kharton, A. P. Viskup, J. R. Frade and V. V. Samakhval, *Journal of the European Ceramic Society*, 2006, **26**, 1371-1378.

173. V. V. Kharton, M. V. Patrakeev, J. C. Waerenborgh, A. V. Kovalevsky, Y. V. Pivak, P. Gaczynski, A. A. Markov and A. A. Yaremchenko, *Journal of Physics and Chemistry of Solids*, 2007, **68**, 355-366.

174. A. Kovalevsky, V. V. Kharton, F. M. M. Snijkers, J. F. C. Cooymans, J. J. Luyten and F. M. B. Marques, *Journal of Membrane Science*, 2007, **301**, 238-244.

175. H. L. Lein, K. Wiik and T. Grande, *Solid State Ionics*, 2006, **177**, 1795-1798.

176. M. Sogaard, P. V. Hendriksen and M. Mogensen, *Journal of Solid State Chemistry*, 2007, **180**, 1489-1503.

177. J. Holc, D. Kuscer, M. Hrovat, S. Bernik and D. Kolar, *Solid State Ionics*, 1997, **95**, 259-268.

178. L. Kindermann, D. Das, H. Nickel, K. Hilpert, C. C. Appel and F. W. Poulson, *Journal of the Electrochemical Society*, 1997, **144**, 717-720.

179. J. H. Wan, J. Q. Yan and J. B. Goodenough, *Journal of the Electrochemical Society*, 2005, **152**, A1511-A1515.

180. M. Al Daroukh, V. V. Vashook, H. Ullmann, F. Tietz and I. A. Raj, *Solid State Ionics*, 2003, **158**, 141-150.

181. H. Uchida, S. Arisaka and M. Watanabe, *Journal of the Electrochemical Society*, 2002, **149**, A13-A18.

182. Y. Teraoka, T. Nobunaga, K. Okamoto, N. Miura and N. Yamazoe, *Solid State Ionics*, 1991, **48**, 207-212.

183. M. Godickemeier, K. Sasaki, L. J. Gauckler and I. Riess, *Solid State Ionics*, 1996, **86-8**, 691-701.

184. S. B. Adler, *Solid State Ionics*, 1998, **111**, 125-134.

185. T. Kawada, K. Masuda, J. Suzuki, A. Kaimai, K. Kawamura, Y. Nigara, J. Mizusaki, H. Yugami, H. Arashi, N. Sakai and H. Yokokawa, *Solid State Ionics*, 1999, **121**, 271-279.

186. R. H. E. van Doorn and A. J. Burggraaf, *Solid State Ionics*, 2000, **128**, 65-78.

187. Y. Takeda, H. Ueno, N. Imanishi, O. Yamamoto, N. Sammes and M. B. Phillipps, *Solid State Ionics*, 1996, **86-8**, 1187-1190.

188. T. Hibino, A. Hashimoto, T. Inoue, J. Tokuno, S. Yoshida and M. Sano, *Science*, 2000, **288**, 2031-2033.

189. L. W. Tai, M. M. Nasrallah, H. U. Anderson, D. M. Sparlin and S. R. Sehlin, *Solid State Ionics*, 1995, **76**, 259-271.

190. G. C. Kostogloudis and C. Ftikos, *Solid State Ionics*, 1999, **126**, 143-151.

191. H. Y. Tu, Y. Takeda, N. Imanishi and O. Yamamoto, *Solid State Ionics*, 1999, **117**, 277-281.

192. S. N. a. P. Ruddlesden, P., *Acta Cryst.*, 1958, **11**, 54-55.

193. M. Zinkevich and F. Aldinger, *Journal of Alloys and Compounds*, 2004, **375**, 147-161.

194. A. V. Kovalevsky, V. V. Kharton, A. A. Yaremchenko, Y. V. Pivak, E. V. Tsipis, S. O. Yakovlev, A. A. Markov, E. N. Naumovich and J. R. Frade, *Journal of Electroceramics*, 2007, **18**, 205-218.

195. R. Sayers, J. Liu, B. Rustumji and S. J. Skinner, *Fuel Cells*, 2008, **8**, 338-343.

196. V. V. Kharton, A. P. Viskup, A. V. Kovalevsky, E. N. Naumovich and F. M. B. Marques, *Solid State Ionics*, 2001, **143**, 337-353.

197. Q. Li, H. Zhao, L. H. Huo, L. P. Sun, X. L. Cheng and J. C. Grenier, *Electrochemistry Communications*, 2007, **9**, 1508-1512.

198. A. J. Jennings and S. J. Skinner, *Solid State Ionics*, 2002, **152**, 663-667.

199. V. V. Kharton, A. P. Viskup, E. N. Naumovich and F. M. B. Marques, *Journal of Materials Chemistry*, 1999, **9**, 2623-2629.

200. S. J. Skinner and J. A. Kilner, 12th International Conference on Solid State Ionics, Halkidiki, Greece, 1999.

201. M. Yashima, M. Enoki, T. Wakita, R. Ali, Y. Matsushita, F. Izumi and T. Ishihara, *Journal of the American Chemical Society*, 2008, **130**, 2762-+.

202. J. M. Bassat, P. Odier, A. Villesuzanne, C. Marin and M. Pouchard, *Solid State Ionics*, 2004, **167**, 341-347.

203. M. Burriel, G. Garcia, J. Santiso, J. A. Kilner, J. C. C. Richard and S. J. Skinner, *Journal of Materials Chemistry*, 2008, **18**, 416-422.

204. G. T. Kim, S. Y. Wang, A. J. Jacobson, Z. Yuan and C. L. Chen, *Journal of Materials Chemistry*, 2007, **17**, 1316-1320.

205. V. V. Kharton, E. V. Tsipis, A. A. Yaremchenko and J. R. Frade, *Solid State Ionics*, 2004, **166**, 327-337.

206. V. V. Kharton, F. M. Figueiredo, L. Navarro, E. N. Naumovich, A. V. Kovalevsky, A. A. Yaremchenko, A. P. Viskup, A. Carneiro, F. M. B. Marques and J. R. Frade, *Journal of Materials Science*, 2001, **36**, 1105-1117.

207. C. N. Munnings, S. J. Skinner, G. Amow, P. S. Whitfield and I. J. Davidson, *Journal of Fuel Cell Science and Technology*, 2005, **2**, 34-37.

208. N. Solak, M. Zinkevich and F. Aldinger, 15th International Conference on Solid State Ionics, Baden Baden, GERMANY, 2006.

209. C. N. Munnings, S. J. Skinner, G. Amow, P. S. Whitfield and L. J. Davidson, *Solid State Ionics*, 2006, **177**, 1849-1853.

210. L. P. Sun, L. H. Huo, H. Zhao, Q. Li and C. Pijolat, *Journal of Power Sources*, 2008, **179**, 96-100.

211. Z. P. Shao, W. S. Yang, Y. Cong, H. Dong, J. H. Tong and G. X. Xiong, *Journal of Membrane Science*, 2000, **172**, 177-188.

212. H. H. Wang, C. Tablet, A. Feldhoff and H. Caro, *Journal of Membrane Science*, 2005, **262**, 20-26.

213. S. McIntosh, J. F. Vente, W. G. Haije, D. H. A. Blank and H. J. M. Bouwmeester, *Chemistry of Materials*, 2006, **18**, 2187-2193.

214. Q. S. Zhu, T. A. Jin and Y. Wang, *Solid State Ionics*, 2006, **177**, 1199-1204.

215. J. Pena-Martinez, D. Marrero-Lopez, J. C. Ruiz-Morales, B. E. Buergler, P. Nunez and L. J. Gauckler, 15th International Conference on Solid State Ionics, Baden Baden, GERMANY, 2006.

216. Q. L. Liu, K. A. Khor and S. H. Chan, *Journal of Power Sources*, 2006, **161**, 123-128.

217. S. Y. Li, Z. Lu, X. Q. Huang and W. H. Su, *Solid State Ionics*, 2008, **178**, 1853-1858.

218. J. G. Thompson, R. L. Withers and F. J. Brink, *Journal of Solid State Chemistry*, 1999, **143**, 122-131.

219. S. J. Skinner, I. J. E. Brooks and C. N. Munnings, *Acta Crystallographica Section C-Crystal Structure Communications*, 2004, **60**, I37-I39.

220. E. V. Tsipis, C. N. Munnings, V. V. Kharton, S. J. Skinner and J. R. Frade, *Solid State Ionics*, 2006, **177**, 1015-1020.

221. R. J. Packer, E. V. Tsipis, C. N. Munnings, V. V. Kharton, S. J. Skinner and J. R. Frade, *Solid State Ionics*, 2006, **177**, 2059-2064.

222. R. J. Packer, S. J. Skinner, A. A. Yaremchenko, E. V. Tsipis, V. V. Kharton, M. V. Patrakeev and Y. A. Bakhteeva, *Journal of Materials Chemistry*, 2006, **16**, 3503-3511.

223. R. J. Packer, J. Barlow, A. Cott and S. J. Skinner, *Solid State Ionics*, 2008, **179**, 1094-1100.

224. F. Vullum and T. Grande, *Chemistry of Materials*, 2008, **20**, 5434-5437.

225. M. Respaud, C. Frontera, J. L. Garcia-Munoz, M. A. G. Aranda, B. Raquet, J. M. Broto, H. Rakoto, M. Goiran, A. Llobet and J. Rodriguez-Carvajal, *Physical Review B*, 2001, **6421**, art. no.-214401.

226. A. Maignan, C. Martin, D. Pelloquin, N. Nguyen and B. Raveau, *Journal of Solid State Chemistry*, 1999, **142**, 247-260.

227. A. A. Taskin, A. N. Lavrov and Y. Ando, *Applied Physics Letters*, 2005, **86**.

228. A. M. Chang, S. J. Skinner and J. A. Kilner, *Solid State Ionics*, 2006, **177**, 2009-2011.

229. A. Tarancon, S. J. Skinner, R. J. Chater, F. Hernandez-Ramirez and J. A. Kilner, *Journal of Materials Chemistry*, 2007, **17**, 3175-3181.

230. N. Li, Z. Lu, B. O. Wei, X. Q. Huang, K. F. Chen, Y. Z. Zhang and W. H. Su, *Journal of Alloys and Compounds*, 2008, **454**, 274-279.

231. J. Pena-Martinez, A. Tarancon, D. Marrero-Lopez, J. C. Ruiz-Morales and P. Nunez, *Fuel Cells*, 2008, **8**, 351-359.

232. J. H. Kim, F. Prado and A. Manthiram, *Journal of the Electrochemical Society*, 2008, **155**, B1023-B1028.

233. G. Kim, S. Wang, A. J. Jacobson, L. Reimus, P. Brodersen and C. A. Mims, *Journal of Materials Chemistry*, 2007, **17**, 2500-2505.

234. G. Kim, S. Wang, A. J. Jacobson, Z. Yuan, W. Donner, C. L. Chen, L. Reimus, P. Brodersen and C. A. Mims, *Applied Physics Letters*, 2006, **88**.

235. C. J. Zhu, X. M. Liu, C. S. Yi, D. Yan and W. H. Su, *Journal of Power Sources*, 2008, **185**, 193-196.

236. Q. J. Zhou, T. M. He and Y. Ji, *Journal of Power Sources*, 2008, **185**, 754-758.

237. T. Z. Sholklapper, V. Radmilovic, C. P. Jacobson, S. J. Visco and L. C. De Jonghe, *Journal of Power Sources*, 2008, **175**, 206-210.

238. P. Datta, P. Majewski and F. Aldinger, *Materials Chemistry and Physics*, 2008, **107**, 370-376.

239. H. Z. Zhang, H. Y. Liu, Y. Cong and W. S. Yang, *Journal of Power Sources*, 2008, **185**, 129-135.

240. S. McIntosh, S. B. Adler, J. M. Vohs and R. J. Gorte, *Electrochemical and Solid State Letters*, 2004, **7**, A111-A114.

241. M. J. L. Ostergard, C. Clausen, C. Bagger and M. Mogensen, *Electrochimica Acta*, 1995, **40**, 1971-1981.

242. M. Juhl, S. Primdahl, C. Manon and M. Mogensen, *Journal of Power Sources*, 1996, **61**, 173-181.

243. E. P. Murray, T. Tsai and S. A. Barnett, *Solid State Ionics*, 1998, **110**, 235-243.

244. V. A. C. Haanappel, J. Mertens, D. Rutenbeck, C. Tropartz, W. Herzhof, D. Sebold and F. Tietz, *Journal of Power Sources*, 2005, **141**, 216-226.

245. A. Princivalle and E. Djurado, *Solid State Ionics*, 2008, **179**, 1921-1928.

246. Y. Y. Huang, J. M. Vohs and R. J. Gorte, *Journal of the Electrochemical Society*, 2006, **153**, A951-A955.

247. Z. W. Wang, M. J. Cheng, Y. L. Dong, M. Zhang and H. M. Zhang, *Solid State Ionics*, 2005, **176**, 2555-2561.

248. A. Hagiwara, N. Hobara, K. Takizawa, K. Sato, H. Abe and M. Naito, *Solid State Ionics*, 2006, **177**, 2967-2977.

249. N. T. Hart, N. P. Brandon, M. J. Day and N. Lapena-Rey, *Journal of Power Sources*, 2002, **106**, 42-50.

250. H. Zhao, L. H. Huo and S. Gao, *Journal of Power Sources*, 2004, **125**, 149-154.

251. Z. Y. Jiang, L. Zhang, K. Feng and C. R. Xia, *Journal of Power Sources*, 2008, **185**, 40-48.

252. Y. Zheng, R. Ran, H. X. Gu, R. Cai and Z. P. Shao, *Journal of Power Sources*, 2008, **185**, 641-648.

253. X. G. Zhang, M. Robertson, S. Yick, C. Deces-Petit, E. Styles, W. Qu, Y. S. Xie, R. Hui, J. Roller, O. Kesler, R. Maric and D. Ghosh, *Journal of Power Sources*, 2006, **160**, 1211-1216.

254. X. D. Zhu, K. N. Sun, N. Q. Zhang, X. B. Chen, L. J. Wu and D. C. Jia, *Electrochemistry Communications*, 2007, **9**, 431-435.

255. M. Bevilacqua, T. Montini, C. Tavagnacco, E. Fonda, P. Fornasiero and M. Graziani, *Chemistry of Materials*, 2007, **19**, 5926-5936.

256. C. J. Zhu, X. M. Liu, D. Xu, D. J. Wang, D. Yan, L. Pei, T. Q. Lu and W. H. Su, *Journal of Power Sources*, 2008, **185**, 212-216.

257. A. Esquirol, J. Kilner and N. Brandon, *Solid State Ionics*, 2004, **175**, 63-67.

258. F. Qiang, K. N. Sun, N. Q. Zhang, X. D. Zhu, S. R. Le and D. R. Zhou, *Journal of Power Sources*, 2007, **168**, 338-345.

259. Y. J. Leng, S. H. Chan and Q. L. Liu, *International Journal of Hydrogen Energy*, 2008, **33**, 3808-3817.

260. J. D. Zhang, Y. Ji, H. B. Gao, T. M. He and J. Liu, *Journal of Alloys and Compounds*, 2005, **395**, 322-325.

261. Y. Lin and S. A. Barnett, *Solid State Ionics*, 2008, **179**, 420-427.

262. J. Chen, F. L. Liang, L. N. Liu, S. P. Jiang, B. Chi, J. Pu and J. Li, *Journal of Power Sources*, 2008, **183**, 586-589.

263. M. Camaratta and E. Wachsman, *Journal of the Electrochemical Society*, 2008, **155**, B135-B142.

264. C. Laberty, F. Zhao, K. E. Swider-Lyons and A. V. Virkar, *Electrochemical and Solid State Letters*, 2007, **10**, B170-B174.

265. W. Zhou, Z. P. Shao, R. Ran, P. Y. Zeng, H. X. Gu, W. Q. Jin and N. P. Xu, *Journal of Power Sources*, 2007, **168**, 330-337.

266. K. Wang, R. Ran, W. Zhou, H. X. Gu, Z. P. Shao and J. M. Ahn, *Journal of Power Sources*, 2008, **179**, 60-68.

267. W. X. Zhu, Z. Lu, S. Y. Li, B. Wei, J. P. Miao, X. Q. Huang, K. F. Chen, N. Ai and W. H. Su, *Journal of Alloys and Compounds*, 2008, **465**, 274-279.

268. S. D. Park, J. M. Vohs and R. J. Gorte, *Nature*, 2000, **404**, 265-267.

269. R. J. Gorte, S. Park, J. M. Vohs and C. H. Wang, *Advanced Materials*, 2000, **12**, 1465-1469.

270. S. W. Jung, C. Lu, H. P. He, K. Y. Ahn, R. J. Gorte and J. M. Vohs, *Journal of Power Sources*, 2006, **154**, 42-50.

271. H. P. He, J. M. Vohs and R. J. Gorte, *Journal of the Electrochemical Society*, 2003, **150**, A1470-A1475.

272. J. R. Wilson and S. A. Barnett, *Electrochemical and Solid State Letters*, 2008, **11**, B181-B185.

273. O. Costa-Nunes, R. J. Gorte and J. M. Vohs, *Journal of Power Sources*, 2005, **141**, 241-249.

274. X. F. Ye, B. Huang, S. R. Wang, Z. R. Wang, L. Xiong and T. L. Wen, *Journal of Power Sources*, 2007, **164**, 203-209.

275. H. Kim, C. Lu, W. L. Worrell, J. M. Vohs and R. J. Gorte, *Journal of the Electrochemical Society*, 2002, **149**, A247-A250.

276. J. C. Ruiz-Morales, J. Canales-Vazquez, D. Marrero-Lopez, J. Pena-Martinez, A. Tarancon, J. T. S. Irvine and P. Nunez, *Journal of Materials Chemistry*, 2008, **18**, 5072-5077.

277. C. Lu, W. L. Worrell, R. J. Gorte and J. M. Vohs, *Journal of the Electrochemical Society*, 2003, **150**, A354-A358.

278. C. Lu, S. An, W. L. Worrell, J. M. Vohs and R. J. Gorte, *Solid State Ionics*, 2004, **175**, 47-50.

279. C. Lu, W. L. Worrell, J. M. Vohs and R. J. Gorte, *Solid Oxide Fuel Cells Viii (Sofc Viii)*, 2003, **2003**, 773-780.

280. C. Lu, W. L. Worrell, C. Wang, S. Park, H. Kim, J. M. Vohs and R. J. Gorte, *Solid State Ionics*, 2002, **152**, 393-397.

281. M. D. Gross, J. M. Vohs and R. J. Gorte, *Journal of the Electrochemical Society*, 2006, **153**, A1386-A1390.

282. A. C. Tavares, B. L. Kuzin, S. M. Beresnev, N. M. Bogdanovich, E. K. Urumchin, Y. A. Dubitsky and A. Zaopo, *Journal of Power Sources*, 2008, **183**, 20-25.

283. T. M. He, P. F. Guan, L. G. Cong, Y. Ji, H. Sun, J. X. Wang and J. Liu, *Journal of Alloys and Compounds*, 2005, **393**, 292-298.

284. S. An, C. Lu, W. L. Worrell, R. J. Gorte and J. M. Vohs, *Solid State Ionics*, 2004, **175**, 135-138.

285. A. Ringuede, J. A. Labrincha and J. R. Frade, *Solid State Ionics*, 2001, **141-142**, 549-557.

286. C. M. Grgicak, R. G. Green and J. B. Giorgi, *J. Mater. Chem.*, 2006, **16**, 885-897.

287. N. Kiratzis, P. Holtappels, C. E. Hatchwell, M. Mogensen and J. T. S. Irvine, *Fuel Cells*, 2001, **1**, 211-218.

288. J. C. Ruiz-Morales, P. Nunez, R. Buchanan and J. T. S. Irvine, *J. Electrochem. Soc.*, 2003, **150**, A1030-A1036.

289. S. W. Tao and J. T. S. Irvine, *Journal of the Electrochemical Society*, 2004, **151**, A252-A259.

290. S. W. Tao and J. T. S. Irvine, *Nature Materials*, 2003, **2**, 320-323.

291. A. Ovalle, J. C. Ruiz-Morales, J. Canales-Vazquez, D. Marrero-Lopez and J. T. S. Irvine, *Solid State Ionics*, 2006, **177**, 1997-2003.

292. P. R. Slater and J. T. S. Irvine, *Solid State Ionics*, 1999, **120**, 125-134.

293. A. Kaiser, J. L. Bradley, P. R. Slater and J. T. S. Irvine, *Solid State Ionics*, 2000, **135**, 519-524.

294. Y. H. Huang, R. I. Dass, Z. L. Xing and J. B. Goodenough, *Science*, 2006, **312**, 254-257.

295. M. Weston and I. S. Metcalfe, *Solid State Ionics*, 1998, **113**, 247-251.

296. A. L. Sauvet and J. Fouletier, *Journal of Power Sources*, 2001, **101**, 259-266.

297. A. L. Sauvet and J. T. S. Irvine, *Solid State Ionics*, 2004, **167**, 1-8.

298. T. Ramos and A. Atkinson, *Solid State Ionics*, 2004, **170**, 275-286.

299. T. Ramos and A. Atkinson, *Ionic and Mixed Conducting Ceramics Iv*, 2002, **2001**, 352-367.

300. E. S. Raj, J. A. Kilner and J. T. S. Irvine, *Solid State Ionics*, 2006, **177**, 1747-1752.

301. S. M. Plint, P. A. Connor, S. Tao and J. T. S. Irvine, *Solid State Ionics*, 2006, **177**, 2005-2008.

302. J. Wan, J. H. Zhu and J. B. Goodenough, *Solid State Ionics*, 2006, **177**, 1211-1217.

303. J. C. Ruiz-Morales, J. Canales-Vazquez, C. Savaniu, D. Marrero-Lopez, P. Nunez, W. Z. Zhou and J. T. S. Irvine, *Physical Chemistry Chemical Physics*, 2007, **9**, 1821-1830.

304. J. C. Ruiz-Morales, J. Canales-Vazquez, C. Savaniu, D. Marrero-Lopez, W. Z. Zhou and J. T. S. Irvine, *Nature*, 2006, **439**, 568-571.

305. J. Canales-Vazquez, M. J. Smith, J. T. S. Irvine and W. Z. Zhou, *Advanced Functional Materials*, 2005, **15**, 1000-1008.

306. C. Reich, A. Kaiser and I. J.T.S., *Fuel cells: From fundamentals to systems*, 2001, **1**, 249-255.

307. P. Holtappels, F. W. Poulsen and M. Mogensen, *Solid State Ionics*, 2000, **135**, 675-679.

308. J. J. Sprague and H. L. Tuller, *Journal of the European Ceramic Society*, 1999, **19**, 803-806.

309. J. Garcia-Barriocanal, A. Rivera-Calzada, M. Varela, Z. Sefrioui, E. Iborra, C. Leon, S. J. Pennycook and J. Santamaria, *Science*, 2008, **321**, 676-680.

310. I. Kosacki, C. M. Rouleau, P. F. Becher, J. Bentley and D. H. Lowndes, *Solid State Ionics*, 2005, **176**, 1319-1326.

311. A. Yamada, Y. Suzuki, K. Saka, M. Uehara, D. Mori, R. Kanno, T. Kiguchi, F. Mauvy and J. C. Grenier, *Advanced Materials*, 2008, **20**, 4124-+.

312. H. Uchida, A. Yasuda and H. Iwahara, *Denki Kagaku*, 1989, **57**, 153-156.

313. H. Uchida, N. Maeda and H. Iwahara, *Solid State Ionics*, 1983, **11**, 117-124.

314. T. Yajima, H. Suzuki, T. Yogo and H. Iwahara, *Solid State Ionics*, 1992, **51**, 101-107.

315. H. Iwahara, T. Yajima, T. Hibino, K. Ozaki and H. Suzuki, *Solid State Ionics*, 1993, **61**, 65-69.

316. T. Hibino, K. Mizutani, T. Yajima and H. Iwahara, *Solid State Ionics*, 1992, **57**, 303-306.

317. T. Pagnier, I. Charrier-Cougoulic, C. Ritter and G. Lucazeau, *European Physical Journal-Applied Physics*, 2000, **9**, 1-9.

318. I. Charrier-Cougoulic, T. Pagnier and G. Lucazeau, *Journal of Solid State Chemistry*, 1999, **142**, 220-227.

319. P. A. Stuart, T. Unno, R. Ayres-Rocha, E. Djurado and S. J. Skinner, *Journal of the European Ceramic Society*, 2009, **29**, 697-702.

320. P. Babilo and S. M. Haile, *Journal of the American Ceramic Society*, 2005, **88**, 2362-2368.

321. K. D. Kreuer, *Annual Review of Materials Research*, 2003, **33**, 333-359.

322. R. Haugsrud and T. Norby, *Journal of the American Ceramic Society*, 2007, **90**, 1116-1121.

323. R. Haugsrud and T. Norby, *Nature Materials*, 2006, **5**, 193-196.

324. R. Haugsrud, B. Ballesteros, M. Lira-Cantu and T. Norby, *Journal of the Electrochemical Society*, 2006, **153**, J87-J90.

325. R. Haugsrud and T. Norby, *Solid State Ionics*, 2006, **177**, 1129-1135.

326. T. Ishihara, H. Matsuda and Y. Takita, *Journal of the Electrochemical Society*, 1994, **141**, 3444-3449.

327. V. Thangadurai, G. N. Subbanna, A. K. Shukla and J. Gopalakrishnan, *Chemistry of Materials*, 1996, **8**, 1302-1306.

328. P. N. Huang and A. Petric, *Journal of the Electrochemical Society*, 1996, **143**, 1644-1648.

329. N. Liu, M. Shi, C. Wang, Y. P. Yuan, P. Majewski and F. Aldinger, *Journal of Materials Science*, 2006, **41**, 4205-4213.

330. A. Petric, P. Huang and F. Tietz, *Solid State Ionics*, 2000, **135**, 719-725.